RHIC/AP/55

Crystalline Beams in Circular Accelerators

I. Introduction

II. Theoretical approaches

beam frame equations of motion

molecular dynamics calculation

III. Conditions for crystallization

strong focusing vs. weak focusing

below transition energy vs. above

IV. Conditions for melting

V. Conclusion

Jie Wei
Xiao-ping Li
Andrew M. Sessler

1/95

* Introduction

crystalline beam : ultimate "cold" beam

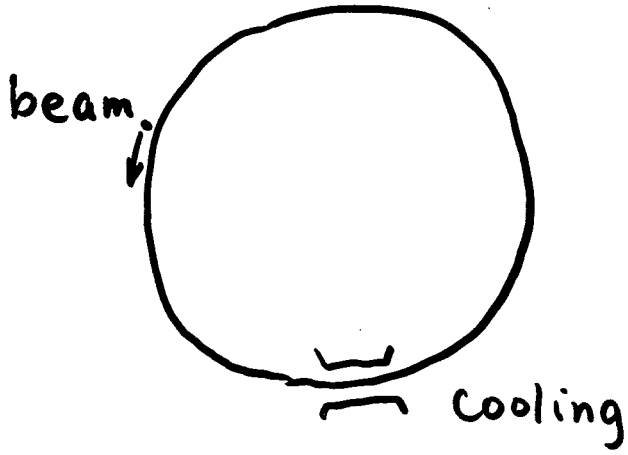

- laser
- electron
- stochastic
- exotic -

focusing force v.s. Coulomb force

⇒ crystalline structure

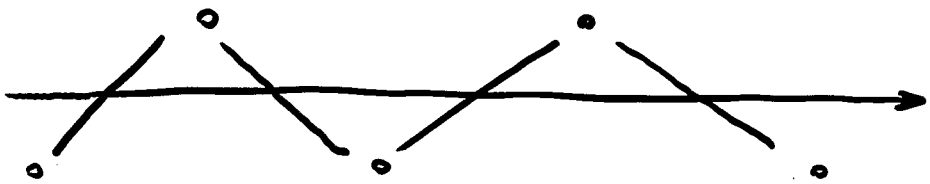

"Coulomb lattice"

"one-component plasma"

History :

1980 Novosibirsk group (Dementiev, et. al.)

see anomaly in cooled proton beam.

1986 Schiffer and Rahman.

theoretical study use MD method

⋮

Habs, Hasse, Avilov, Hoffmann, Hangst.

1988 Gilbert, Bollinger, Wineland

observe layered structure of ions

in penning trap

1993 Wei, Li, Sessler

study actual storage ring, rest frame EOM

⋮ conditions for crystallization & melting

current Experiments (laser cooling), Arhus, Heidelburg

Italian proposal for a dedicated ring.

Okamoto, Sessler, Möhl, 3-D laser cooling

Novosibirsk experiment

NAP - M proton beam. electron cooling

65 MeV. (E_t = 110 MeV)

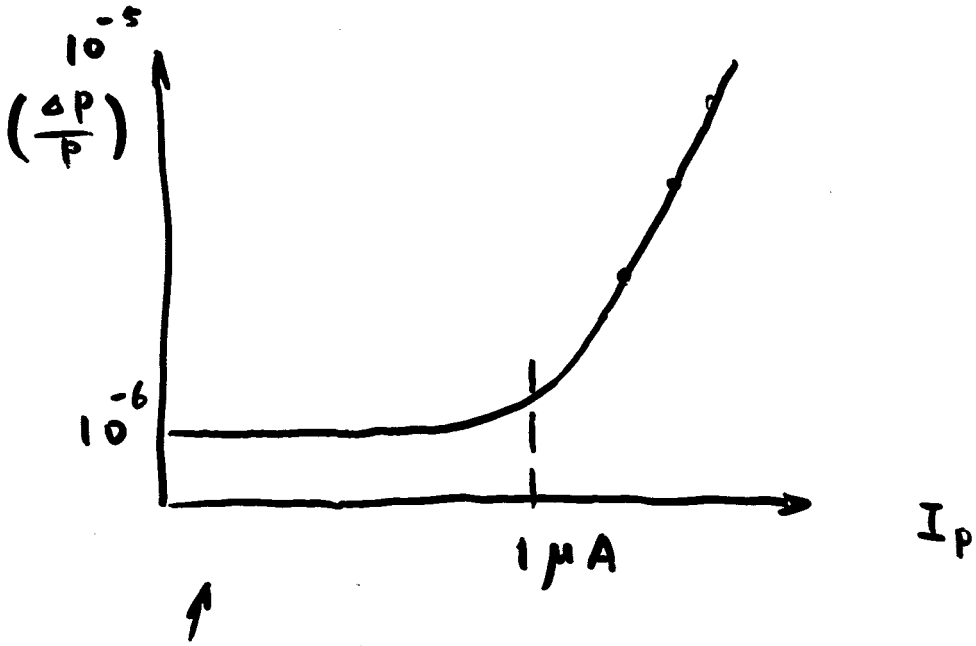

can not be explained by intrabeam scattering theory

E. Dementiev, et. al.

Sov. Phys. Tech. Phys. 25 1001 (1980).

"Anomalous Schottky Signals from a Laser-Cooled Ion beam"

J. S. Hangst, et. al. (Aarhus, Denmark)

Phys. Rev. Lett. 74 86 (1994)

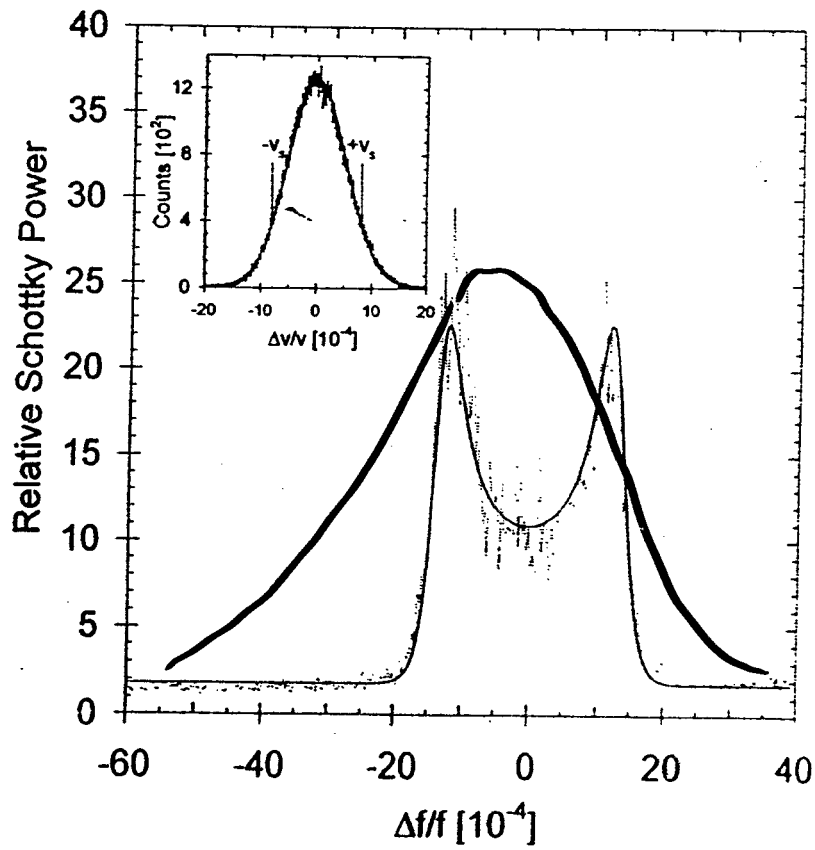

FIG. 1. Measured Schottky signal for the uncooled beam. The solid line is a fit to the theoretical model from Ref. [3]. The inset shows the Gaussian velocity distribution measured by laser fluorescence. The characteristic velocities $\pm v_s$ for charge density waves are indicated.

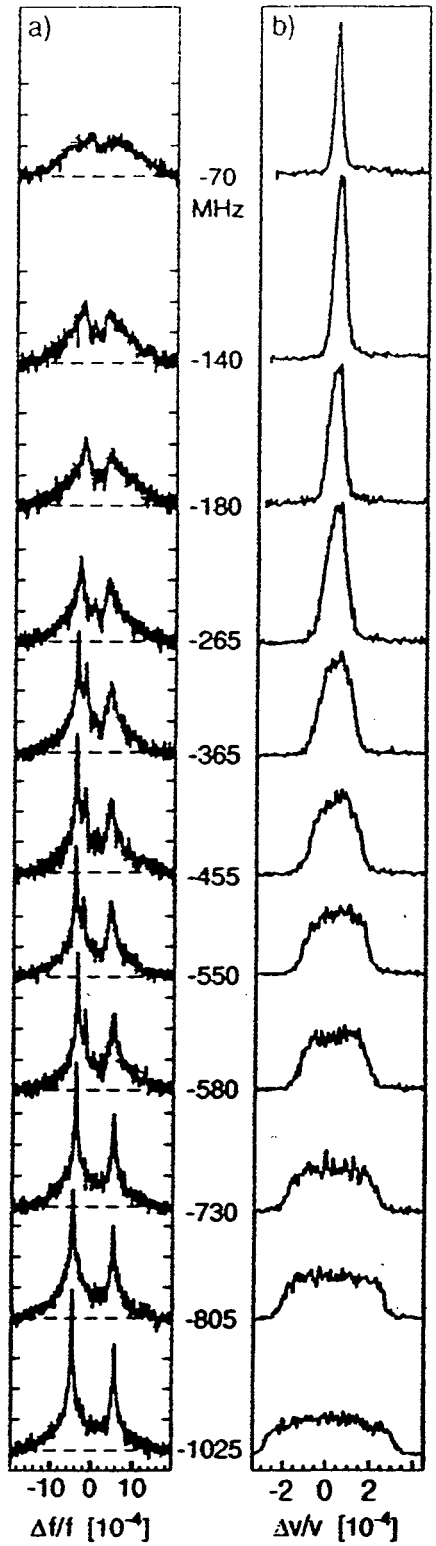

J. S. Hangst et. al.

PRL 74 86 (1995)

FIG. 3. (a) Schottky spectra measured at various detunings (shown between figures) during laser cooling. Dashed lines indicate the noise floor of the measurement; each vertical tick mark is one decade in relative power. The asymmetry in peak heights is probably due to a slight difference in laser powers, leading to larger diffusion past one laser. The nonzero resistivity of the vacuum chamber may also play a role. (b) The corresponding velocity distributions, measured by LIF. Each spectrum contains about 10^3 fluorescence counts.

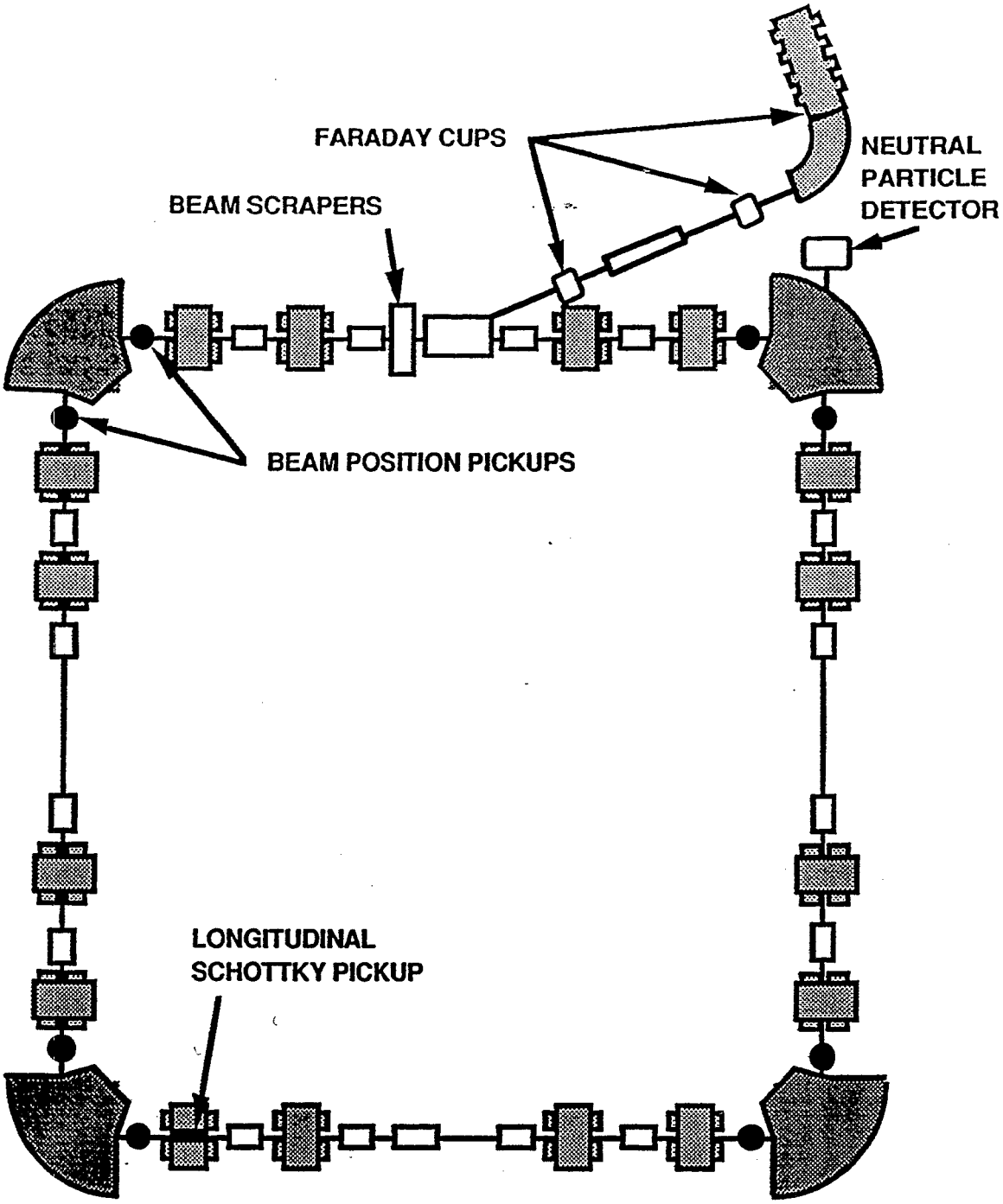

Figure 5-3 ASTRID diagnostic systems

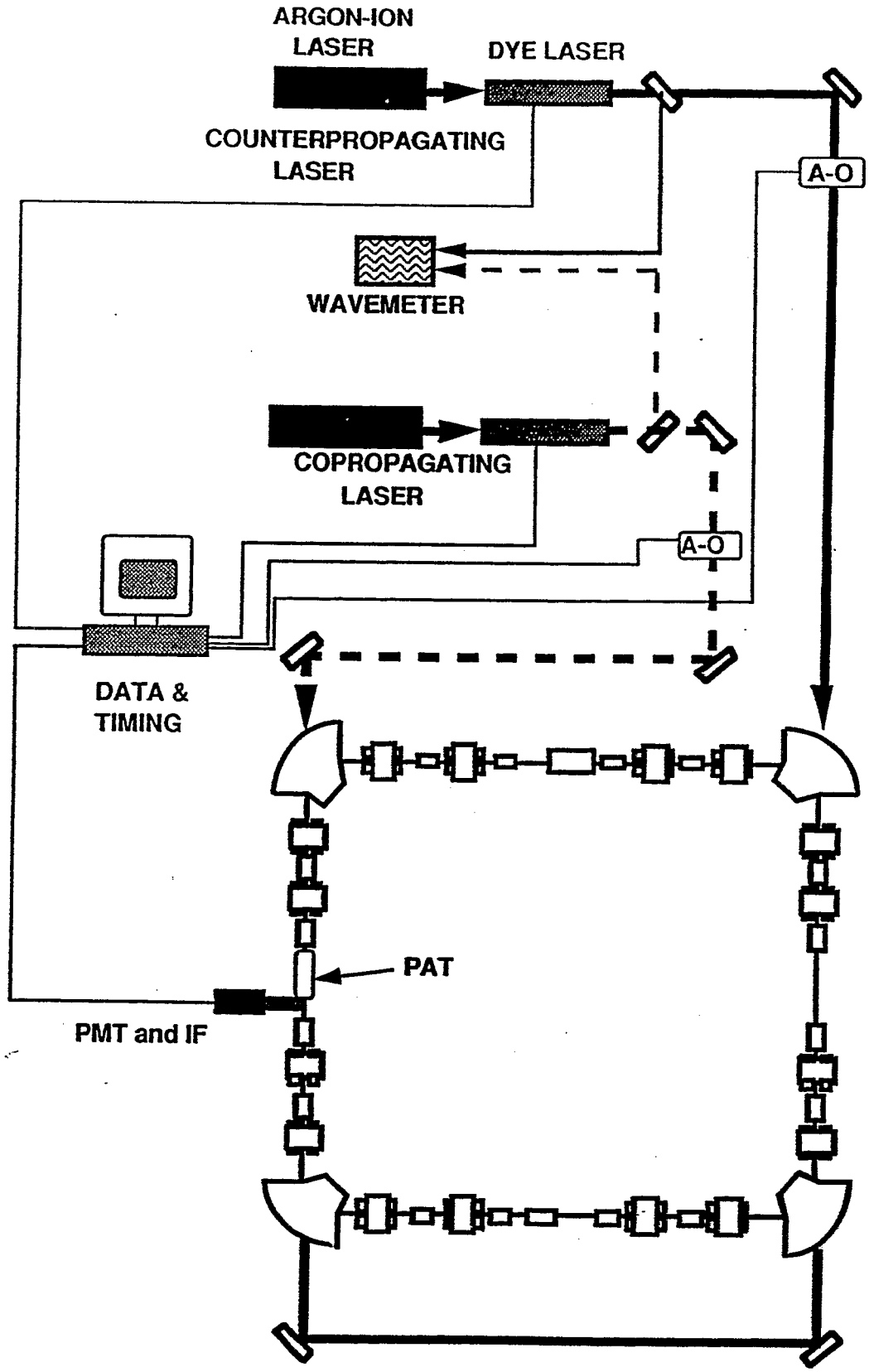

Figure 5-10 ASTRID laser systems

Table 5-1
ASTRID Design Parameters

Circumference	40 m
Length of Straight Sections	7.83 m
Vacuum Chamber Diameter	100 mm
Maximum Magnetic Rigidity	1.87 T-m
Betatron Tunes: Vertical	2.73
Horizontal	2.29
Transition γ	4.58
Chromaticities: Vertical	-7.5
Horizontal	-3.4
Betatron Acceptances: Vertical	60 π mm-mrad
Horizontal	320 π mm-mrad

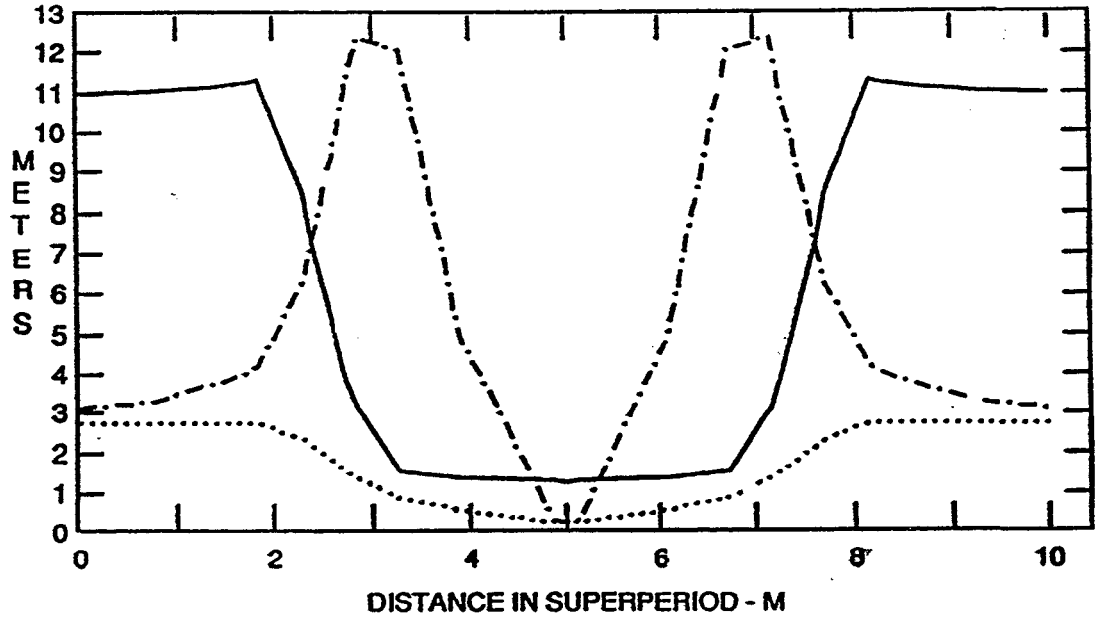

Figure 5-2 ASTRID lattice functions for one superperiod (one-fourth of the ring) ; solid line -β_x*, dot-dashed line -*β_y*, dotted line-*η_x

"Three dimensional Laser cooling of Stored and Circulating Ion Beams by Means of a Coupling Cavity"

H. Okamoto, A.M. Sessler, D. Möhl

Phys. Rev. Lett. 72 3977 (1994)

"Low-energy states of Circulating Stored Ion Beams: crystalline Beams"

J. Wei, X-P. Li, A.M. Sessler

Phys. Rev. Lett. 73 3089 (1994)

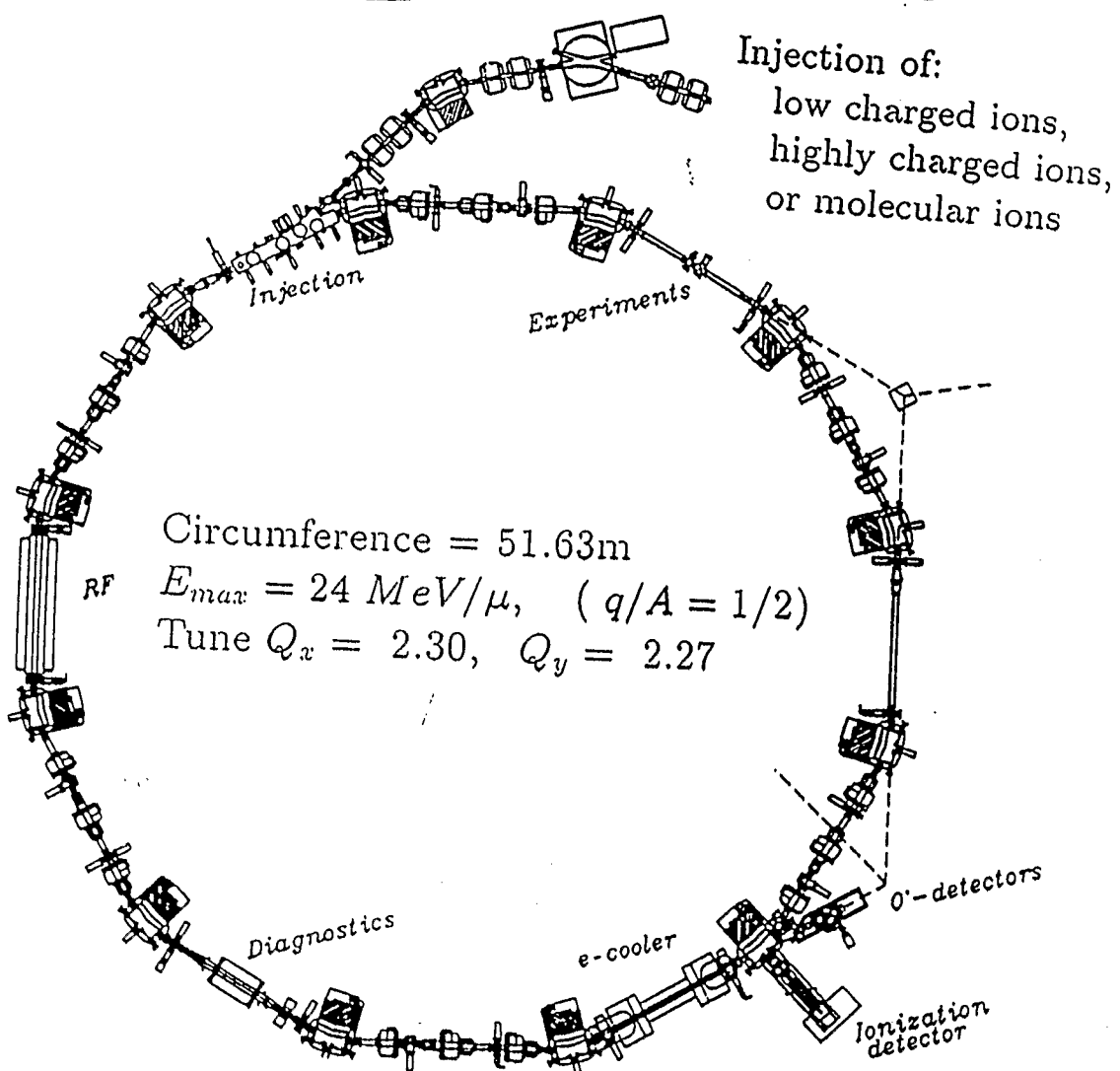

Fig. 1. Layout of the CRYRING facility.

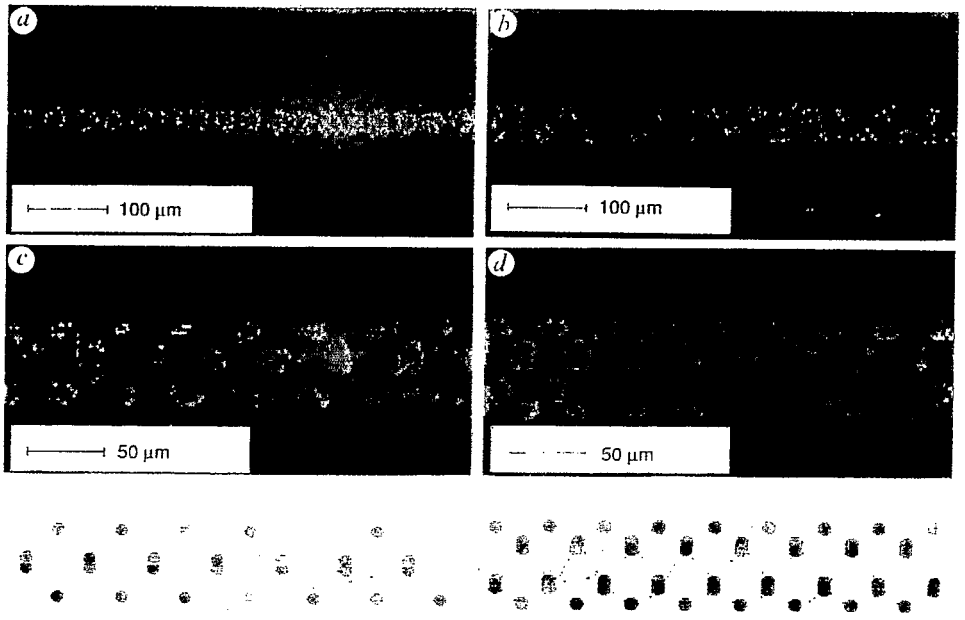

FIG 2 Colour-coded images of crystalline structures of laser-cooled $^{24}Mg^+$ ions. The intensity increases from violet to blue, yellow and red. Individual ions could be resolved in these images The ions arrange themselves in minimum energy configurations. *a*, For low ion density ($\lambda = 0.29$) the ions form a string along the field axis; *b*, increasing the ion density changes the configuration to a zig-zag ($\lambda = 0.92$). At still higher ion densities the ions form ordered helical structures on the surface of a cylinder: *c*, two interwoven helices at $\lambda = 1.9$; *d*, three interwoven helices at $\lambda = 2.6$. Experimental images are displayed above, visualizations below.

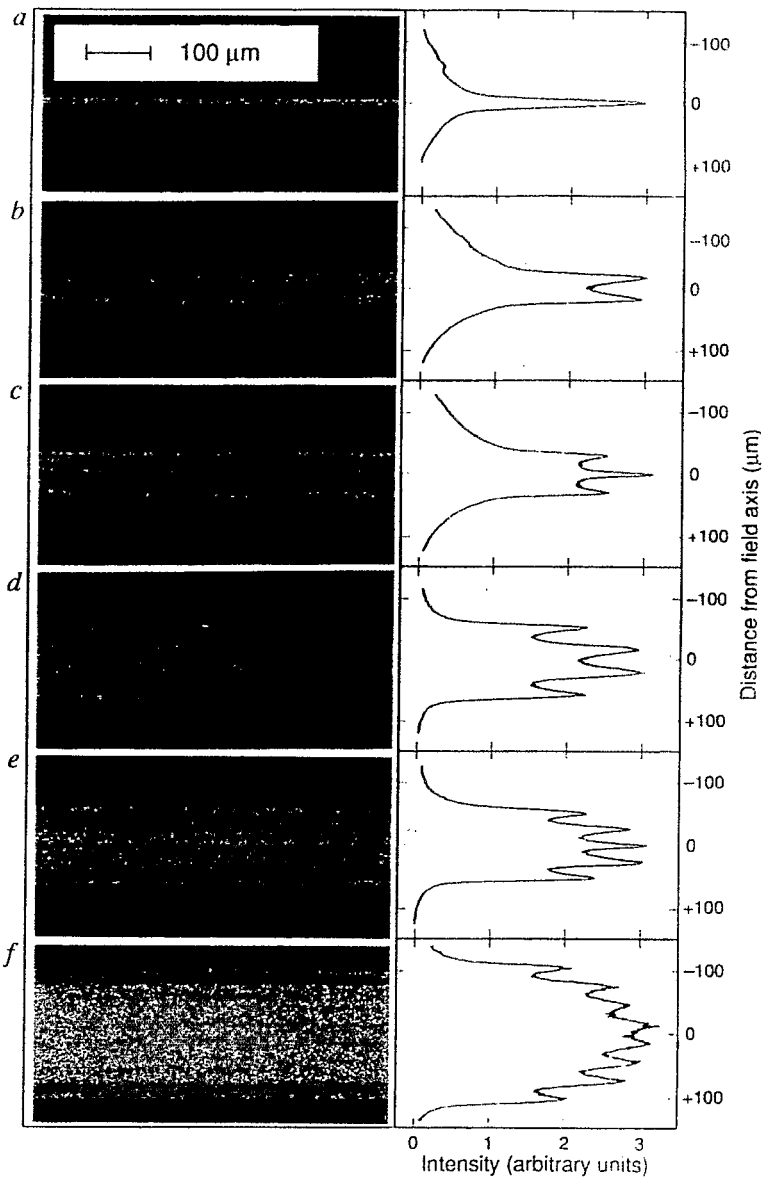

FIG. 3 Images and intensity profiles of (*a*) string, (*b*) one shell ($\rho/a = 1.05$, total ion number in the ring $N \approx 5 \times 10^4$), (*c*) one shell plus string ($\rho/a = 1.8$, $N \approx 1 \times 10^5$), (*d*) two shells ($\rho/a = 2.7$, $N \approx 2 \times 10^5$), (*e*) two shells plus string ($\rho/a = 3.4$, $N \approx 3 \times 10^5$) and (*f*) four shells ($\rho/a = 6.2$, $N \approx 8 \times 10^5$). The ions are not individually resolved. The structures can be identified with the help of the radial intensity profiles (right). The images are colour-coded as in Fig. 2. Integration times are longer than 3 min each.

G. Birkl et.al.

leads to a harmonic confining potential[14] of the form $\psi = \psi_0 r^2/r_0^2$ with the potential depth $\psi_0 = q^2 U_{RF}^2/4m\Omega^2 r_0^2$, where q is the ion charge, m the ion mass, r the distance from the field axis and r_0 half the distance between opposite electrodes. The oscillation frequency in this harmonic potential, $\omega_{sec} = (2\psi_0/mr_0^2)^{1/2}$,

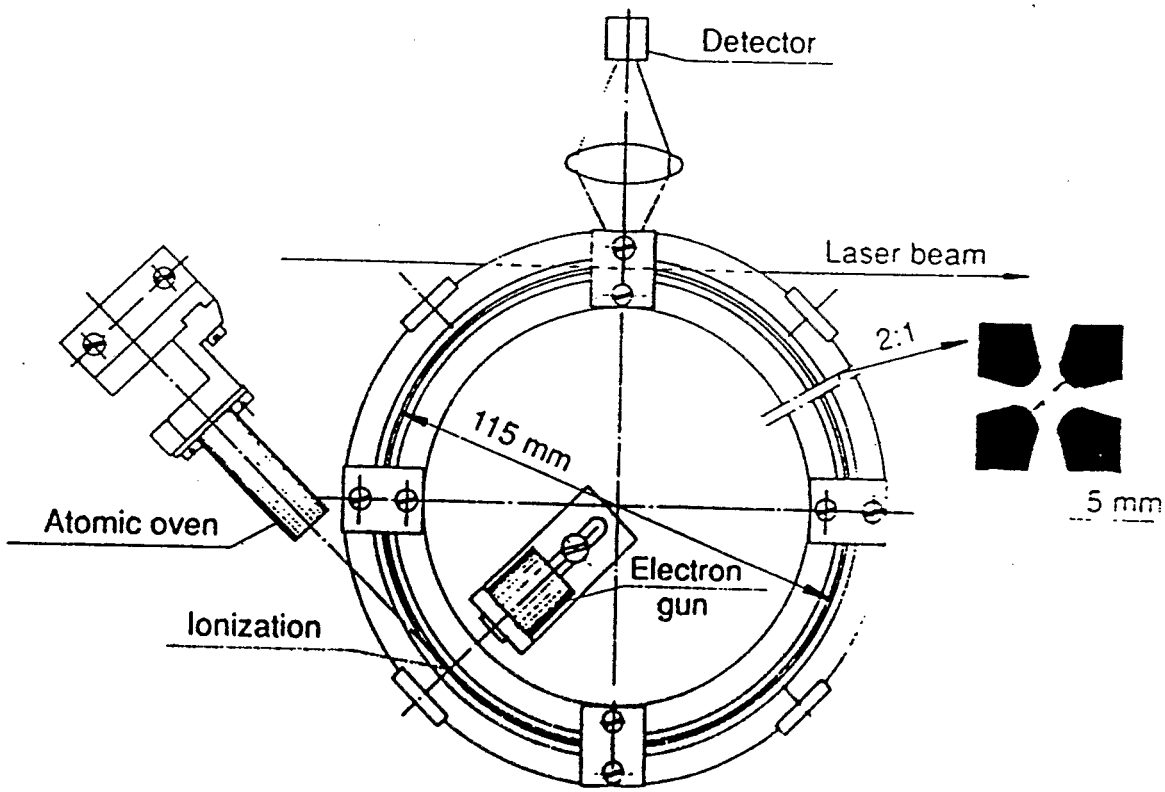

FIG. 1 Quadrupole storage ring, with the atomic beam oven and electron gun. The storage ring consists of four circular electrodes, and the diameter of the toroidal storage volume is $2R = 115$ mm. The insert shows an enlarged cross-section with opposite electrodes having a separation of $2r_0 = 5$ mm. The laser beam enters the storage volume tangentially. Resonance fluorescence is detected with a photomultiplier tube or an imaging photon detector system.

Multiple-shell structures of laser-cooled $^{24}Mg^+$ ions in a quadrupole storage ring

G. Birkl, S. Kassner & H. Walther

Max-Planck-Institut für Quantenoptik, Garching bei München, Germany

THE possibility of creating ordered ion beams in high-energy storage rings[1,2] by means of electron and laser cooling has opened up a new era in accelerator physics. The enhanced luminosity and suppressed momentum spread in such systems create the highest possible phase-space density. The first experimental results were obtained by cooling $^7Li^+$ beams to temperatures of a few kelvin or even to sub-kelvin temperatures[3,4], and the ordered structures have been studied theoretically[5–7] by methods of molecular dynamics. Predicted configurations for the lowest ion densities have been observed in low-energy quadrupole storage rings[8] and linear traps[9]. Recently we showed that at slightly higher ion densities helical structures are obtained[10]. Here we present a series of new experimental results on ordered ion structures in a quadrupole storage ring. In order of increasing ion number, a linear chain of ions, a zig-zag structure, helical structures and finally multiple concentric shells could be observed. The experimental results agree with molecular dynamics calculations.

When ordered structures in storage rings are simulated[5–7], a cylindrically symmetric, static harmonic potential is usually assumed to describe the confining field. The pseudopotential of a low-energy quadrupole storage ring is closer to the theoretical model than the confining field of a high-energy storage ring, where the ions are subjected to periodic squeezing and pulling in the focusing sections, Coulomb explosion in the drift sections and shear forces in the bending sections. The principle and first realizations of quadrupole storage rings are described in refs 11–13. In the ring the ions can move freely along the axis of the quadrupole field and are radially confined by applying a

crystalline structure

1-D

2-D

breathing

increasing density

$\nu_x^2 - \gamma^2$

ν_y^2

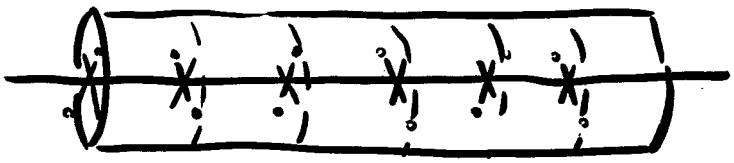

3-D breathing

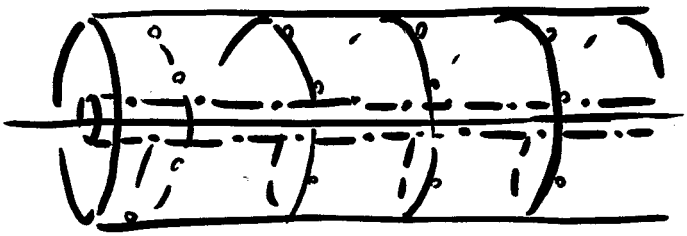

3-D breathing multi-layer

Motivation :

Condensed Matter Physics

1. Systematic (relatively easy to control) study of transition from 1D to 2D to 3D in the ground state; i.e., a careful study of the change in symmetries associated with change of density and with (easily changed) focusing.

2. Study of transport properties in the crystal.

3. Study of the stochasticity temperature. Special to beams vs. particles in traps. Stochasticity for a many-body system vs. usual 1 particle stochasticity studies.

4. Study of a suspended phase; interaction of a solid with a "gas" phase (A special aspect is that the gas phase (especially) absorbs heat at a steady rate from the lattice).

5. Study of phase transitions (sharp or not?) in this system (which could, well, be different than the situation in traps).

6. A new state of matter.

Accelerator Physics

1. In the course of getting crystals have learned many things that are useful more generally:
    1. How to do laser cooling, with two lasers, induction units, RF cavities, etc
    2. How to cool in three dimensions.
    3. How to measure velocity distributions using fluorescence.
    4. New methods of laser cooling (like adiabatic fast passage) are being considered.

2. Very fine beams should be useful for a variety of things such as, (after extraction) for very fine fabrication of semi-conductors (ion implant), to study nuclear levels that are close together (but can't use thick targets because of Landau straggling), for atomic physics (marginal, channeling is a possibility).

3. Development of diagnostic techniques for crystalline beams (Schottky scans, etc.) will be generally useful.

4. Study of intra-beam scattering and various instabilities in a controlled environment.

5. Useful for high luminosity colliders?

Questions :

* Does the crystalline structure exist ?
* What are the effects of shearing.

  AG focusing, straight / bending section ?
* What are the ground-state structures ?
* What machine is most suitable ?
* How long can a crystal last ?
* What is the "melting temperature" ?
* What cooling method can be used ?

II. Theoretical approaches

* derive equations of motion in beam rest fram

* use molecular dynamics method for simulatio

Equations of motion in beam rest fram

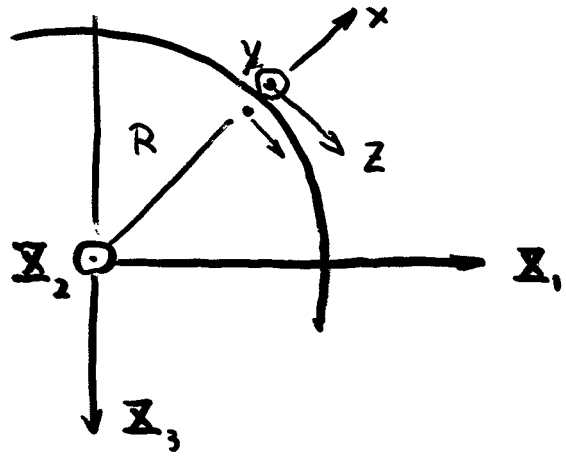

* non-relativistic motion in the rest fram
* straightforward to adopt MD method
* crystallization : $\dot{x} = \dot{y} = \dot{z} = 0$

Derivation:

* use general relativity formalism, EOM in tensor form
* find the transformation
* EOM in lab frame $\Rightarrow$ EOM in rest fram

* Hamiltonian

$$H(x, P_x, y, P_y, z, P_z, t) = \frac{1}{2}(P_x^2 + P_y^2 + P_z^2) - \gamma x P_z + \frac{1}{2}[(1-n)x^2 + n y^2] + V_c$$

$$V_c = \frac{1}{\beta^2\gamma^2}\sum_j \frac{1}{r_j}, \qquad r_j^2 = (x_j - x)^2 + (y_j - y)^2 + (z_j - z$$

$$\begin{cases} \dot{x} = P_x \\ \dot{y} = P_y \\ \dot{z} = P_z - \gamma x \end{cases} \qquad \begin{aligned} \dot{P}_x &= \gamma P_z - (1-n)x - \frac{\partial V_c}{\partial x} \\ \dot{P}_y &= -n y - \frac{\partial V_c}{\partial y} \\ \dot{P}_z &= -\frac{\partial V_c}{\partial z} \end{aligned}$$

* Relation to the lab. frame

$$(P_x, P_y, P_z) = \frac{R}{\xi}\left(x', y', \frac{\Delta p}{p}\right)$$

rest frame lab frame

$$\xi = \left(\frac{r_0 R^2}{\beta^2\gamma^2}\right)^{1/3}, \qquad r_0 = Z^2 e^2 / A m_0 c^2$$

For straight section: (Non-bending, but focusing)

$$\dot{x} = P_x \qquad \dot{P}_x = -\frac{\partial V_c}{\partial x} + n x$$

$$\dot{y} = P_y \qquad \dot{P}_y = -n y - \frac{\partial V_c}{\partial y}$$

$$\dot{z} = P_z \qquad \dot{P}_z = -\frac{\partial V_c}{\partial z}$$

* Molecular dynamics and numerical results

* long-range force. Ewald-type summation

Coulomb potential includes image charges

assume perfectly conducting long pipe

$$\phi(x_i, x_j) = \frac{1}{r_{ij}} + \frac{4}{L}\int_0^\infty \frac{\cosh(2 z_{ij} k/L) J_0(2 \rho_{ij} k/L) - 1}{\exp(2k) - 1} dk$$

$$+ \frac{2}{L}\left[\log(\pi b/L) + C\right].$$

* 1-D periodic condition in azimuthal direction

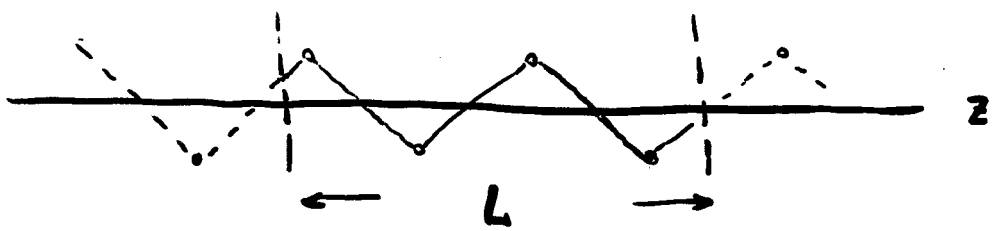

* integrate the equations of motion

4 th order Runge-Kutta algorithm

potential by 15 th order Gauss-Laguerre

* start with random distribution. impose

periodic requirement and drift correction

to reach ground state

storage ring model:

$$\begin{cases} B_x = B_1 \, y \\ B_y = B_0 + B_1 \, x \\ B_z = 0 \end{cases}$$

$\Rightarrow$ reference orbit

$$Z e B_0 R = m_0 c^2 \beta \gamma$$

* equations of motion (in reduced units)

$$\begin{cases} \ddot{x} - \gamma \dot{z} + (-\gamma^2 + 1 - n) x = -\dfrac{\partial V_c}{\partial x} \\ \ddot{y} + n y = -\dfrac{\partial V_c}{\partial y} \\ \ddot{z} + \gamma \dot{x} = -\dfrac{\partial V_c}{\partial z} \end{cases}$$

$n = -\dfrac{B_1 R}{B_0}$ focusing strength

$$\begin{cases} \text{time } t \text{ in unit of } \dfrac{R}{\beta \gamma c} \\ \text{spacial coordinates in } \xi \equiv \left(\dfrac{r_0 R^2}{\beta^2 \gamma^2} \right)^{1/3} \\ \text{energy in } \dfrac{\beta^2 \gamma^2 Z^2 e^2}{\xi} \end{cases}$$

$r_0 = \dfrac{Z^2 e^2}{m_0 c^2}$

III. Conditions for crystallization

1. Weak-focusing machine

constant focusing strength

$$0 < n < 1$$

without Coulomb force

$$\begin{cases} \ddot{x} + (1-n)\,x = 0 \\ \ddot{y} + n\,y = 0 \\ \dot{z} + \gamma x = \text{const.} \end{cases}$$

magnetic quadrupole $\Rightarrow$ horizontal defocusing
vertical focusing

centrifugal force $\Rightarrow$ horizontal focusing

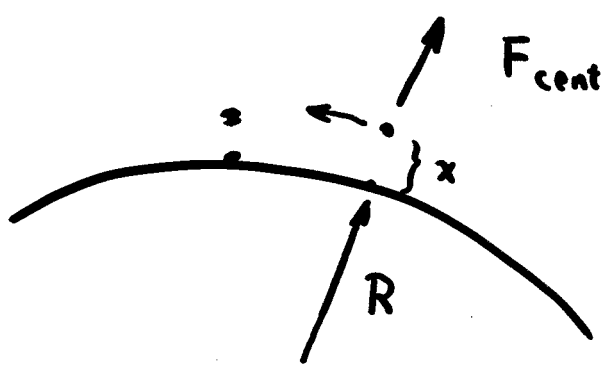

$$F_{cent.} \sim m \frac{v^2}{(R+x)}$$

with Coulomb force & crystallization

$$\begin{cases} \ddot{x} + (-\gamma^2 + 1 - n)\, x = -\dfrac{\partial V_c}{\partial x} \\ \ddot{y} + n\, y = -\dfrac{\partial V_c}{\partial y} \\ \dot{z} \cong 0 , \end{cases}$$

centrifugal force ⇒ horizontal defocusin

$F_{cent.} \sim m\,\omega^2 \cdot (R + x)$

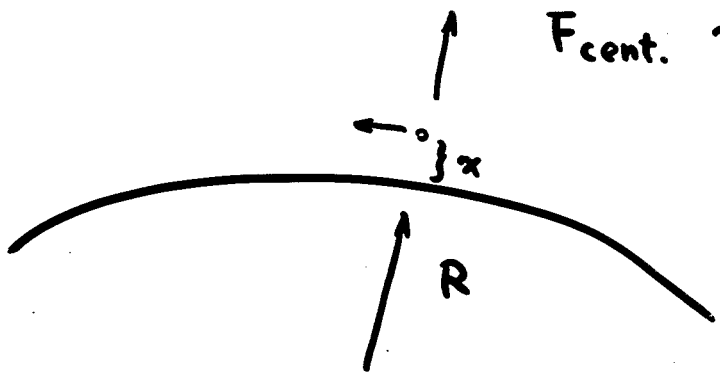

* 3-D crystalline structure can not exist in weak-focusing machine for lack of stability
* 1-D and 2-D structure can not exist either.

Example : 2-D structure can not exist in weak-focusing machine

consider a perturbation on a particle at $z_0 = 0$.

$$\begin{cases} \dot{x} = P_x \\ \dot{P}_x = \gamma P_z - (1 - n - C_x)\, x \\ \dot{z} = P_z - \gamma x \\ \dot{P}_z = -C_z z \end{cases}$$

$$C_x = \sum_j \frac{1}{r_j^3} > 0, \qquad C_z = \sum_j \frac{1}{r_j^3} \left(\frac{3 z_j^2}{r_j^2} - 1 \right)$$

eigenvalue problem

stability :

$$\begin{cases} \gamma^2 - 1 \le -n - C_x & \text{(H)} \\ 0 \le n & \text{(V)} \end{cases}$$

not possible ! $\gamma > 1$.

2. AG focusing machine

stability conditions

kinematic

$$\begin{cases} \nu_x^2 - \gamma^2 > \sum_j \left(\frac{1}{r_j^3} - \frac{3(x_i - x_j)^2}{r_j^5} \right) \\ \nu_y^2 > \sum_j \left(\frac{1}{r_j^3} - \frac{3(y_i - y_j)^2}{r_j^5} \right) \end{cases}$$

(for γ near γ_T)

* crystalline structure can exist only when the beam is below transition energy, $\gamma < \gamma_T$

$\gamma < \gamma_T$

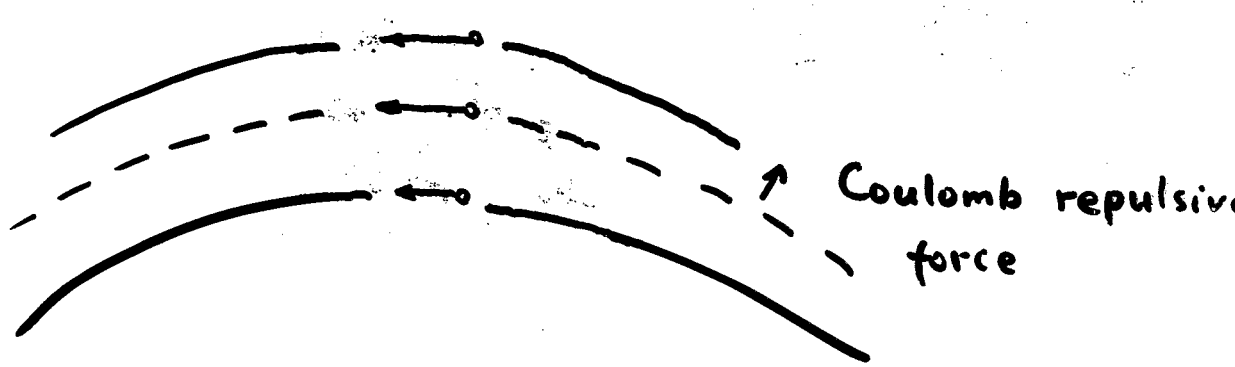

$$\ddot{x} + (\nu_x^2 - \gamma^2)x + F_c = 0$$

* effect of AG focusing

the crystal "breathes" with the lattice

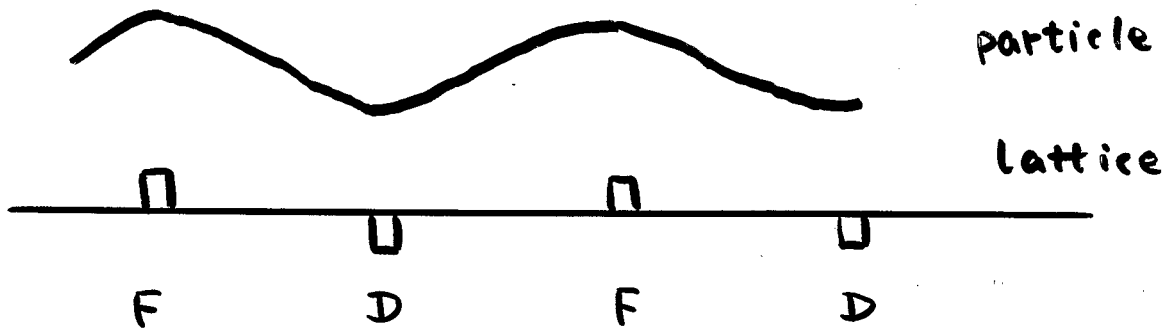

* effect of shear (bending - straight)

the crystal "stretches" with the lattice

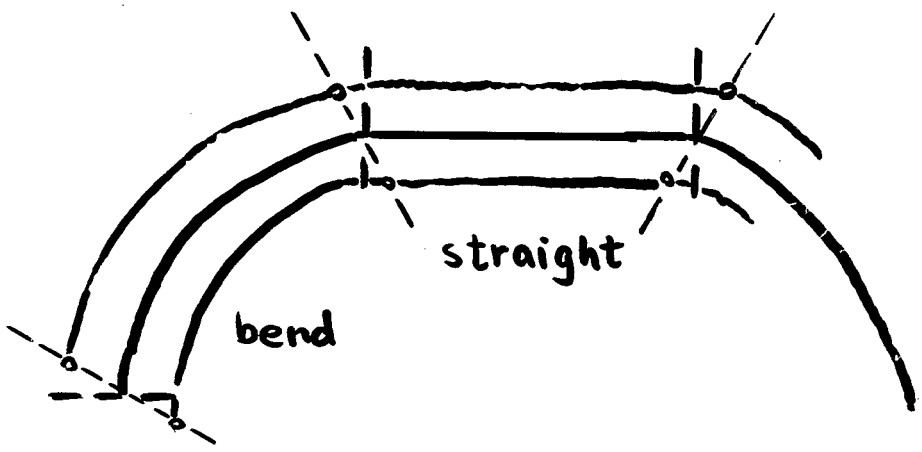

Constant Bending

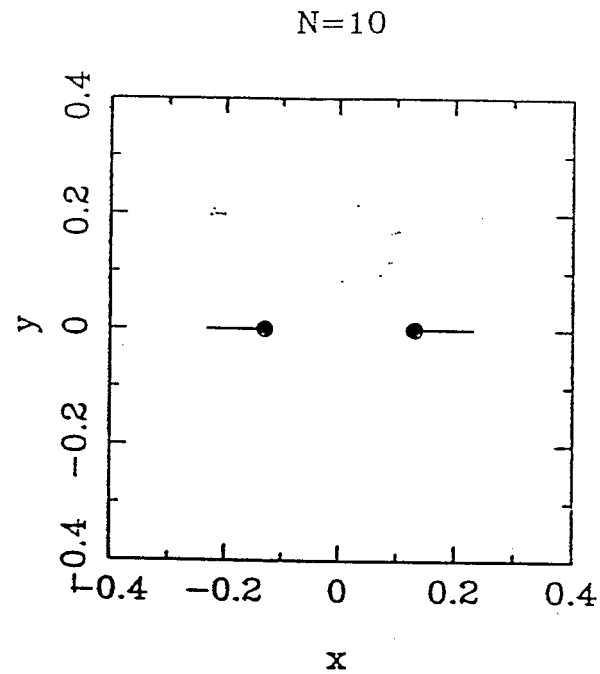

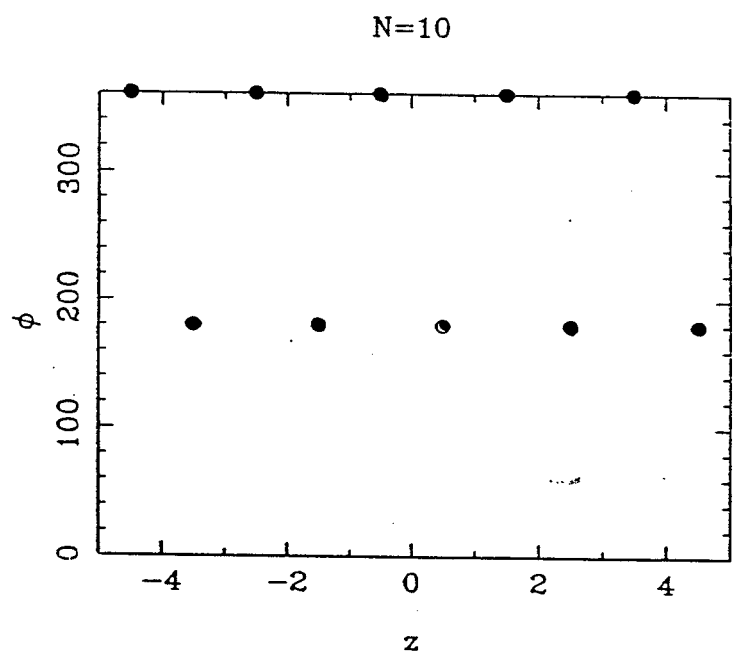

Fig. 2

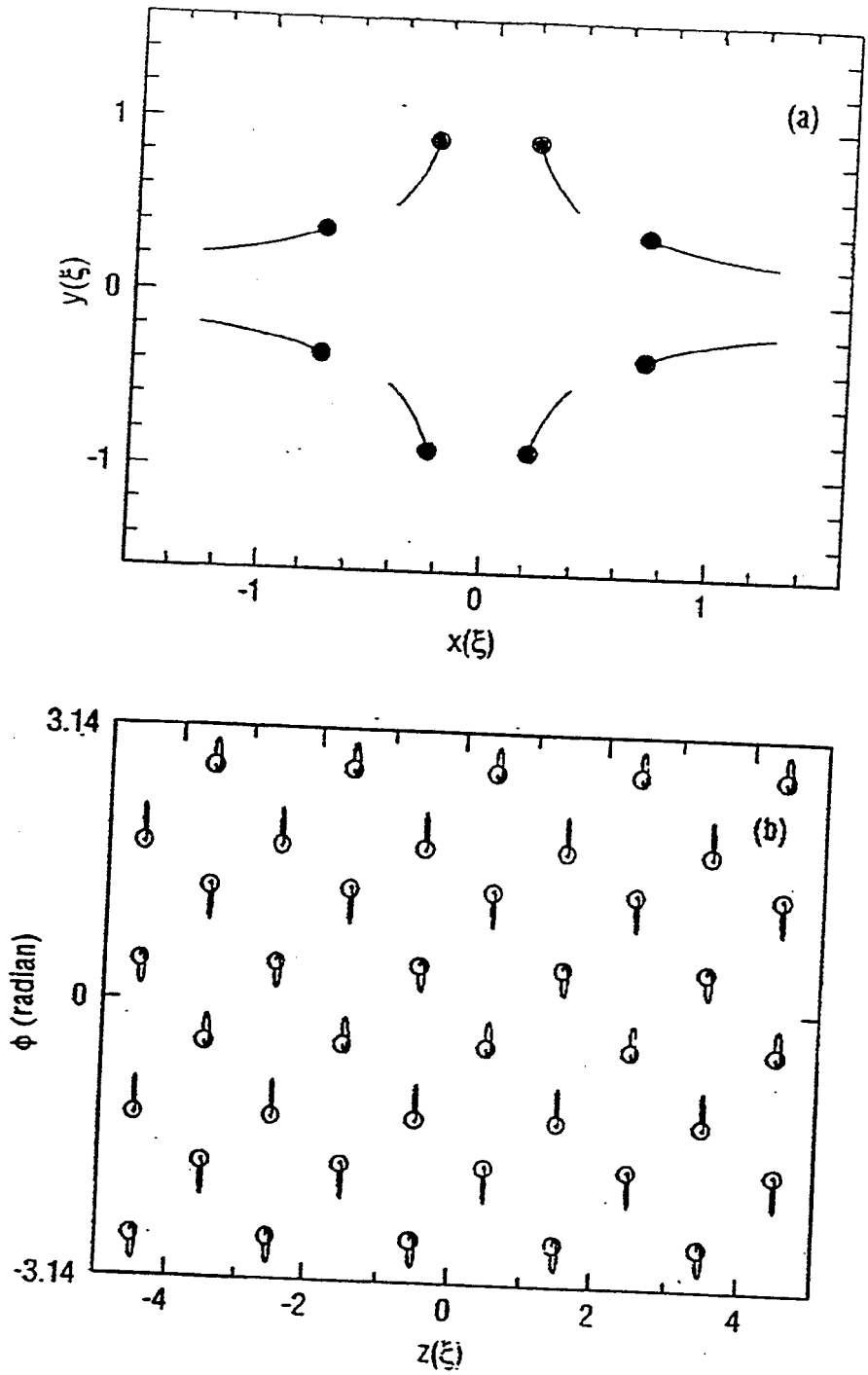

Figure 1: A single-shell structure with particle positions projected (a) into the $x-y$ plane and (b) into the $\phi - z$ plane, where ϕ is the polar angle. The machine consists of 10 FODO (focusing, open or drift, defocusing, open or drift) cells with constant bending with $\nu_x = 2.7$ and $\nu_y = 2.3$, and the particle energy is $\gamma = 1.4$. The number of particles (N) per MD super-cell is 40 and the MD super-cell length (L) is 10ξ. The particles move periodically in time, with the solid lines showing their trajectories and the circles indicating their positions at the start and end of each lattice period.

effect of AG focusing

Constant Bending
N = 60, L = 10

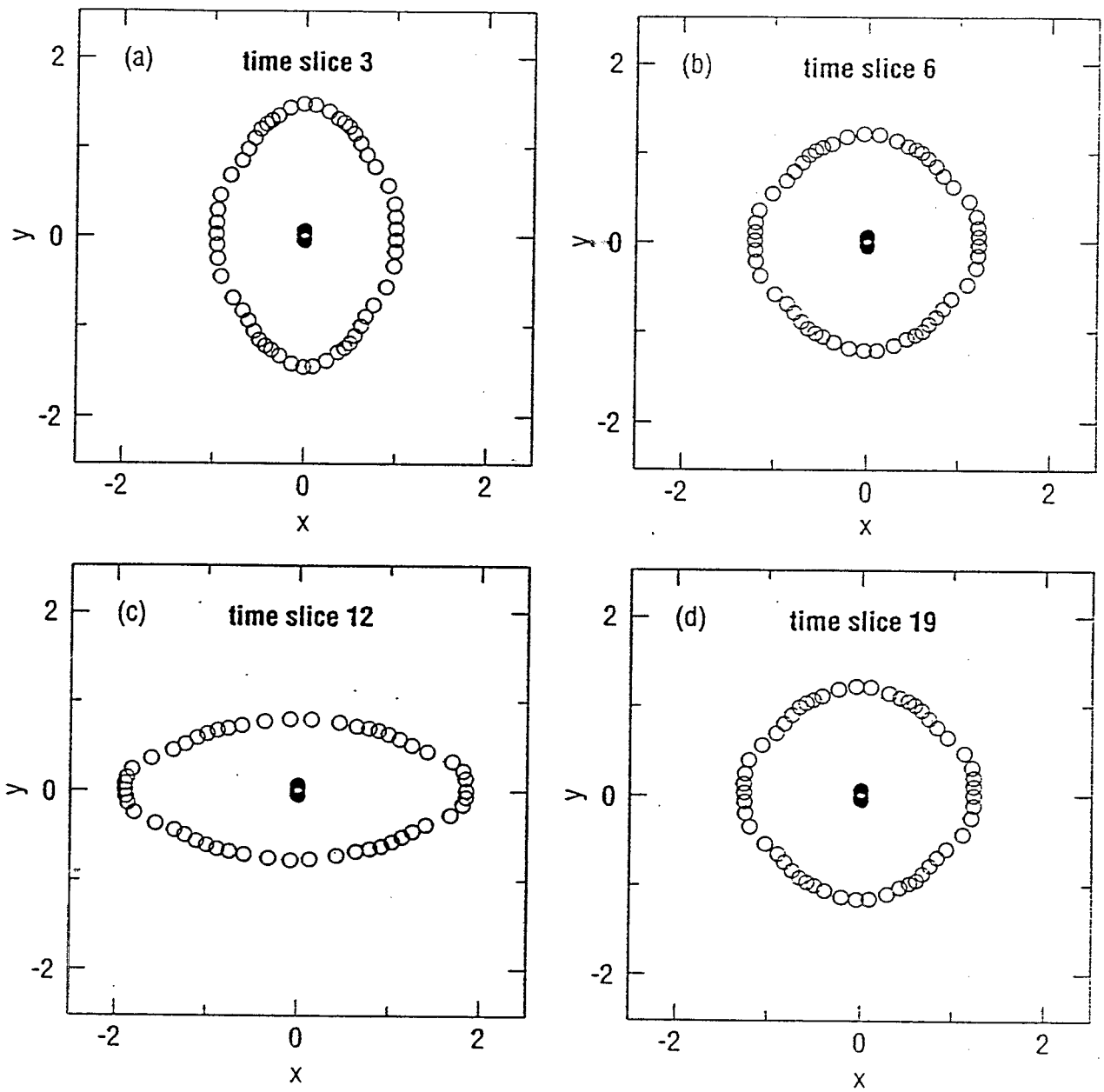

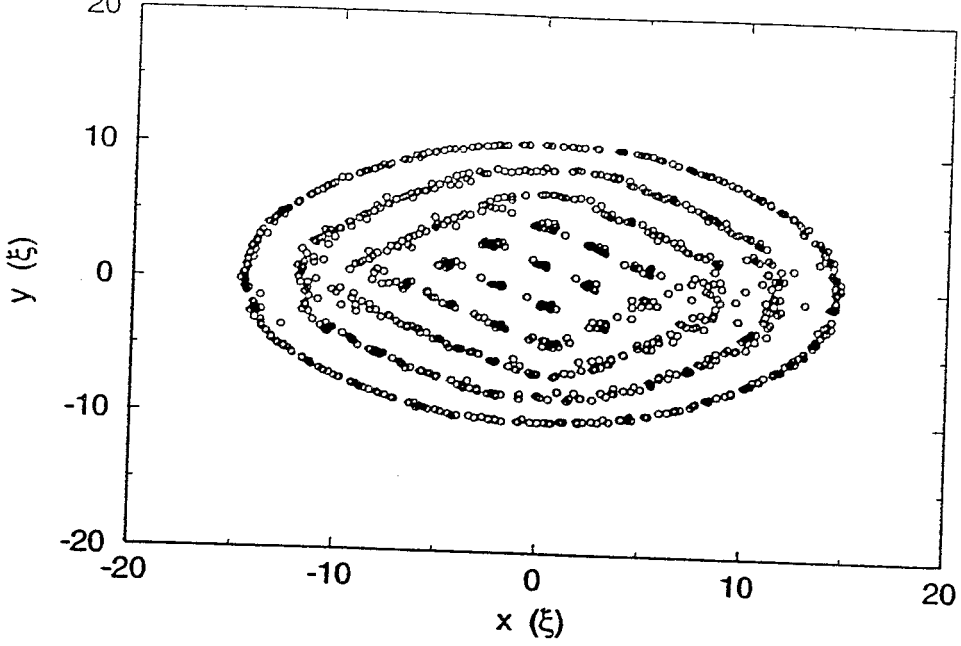

Figure 2: A multi-shell structure with particle positions projected into the $x-y$ plane. The machine consists of 10 FODO cells with 25% bending with $\nu_x=2.8$, $\nu_y=2.1$, and the particle energy is $\gamma=1.4$. The calculation is done with $N=1000$ and $L=40\xi$.

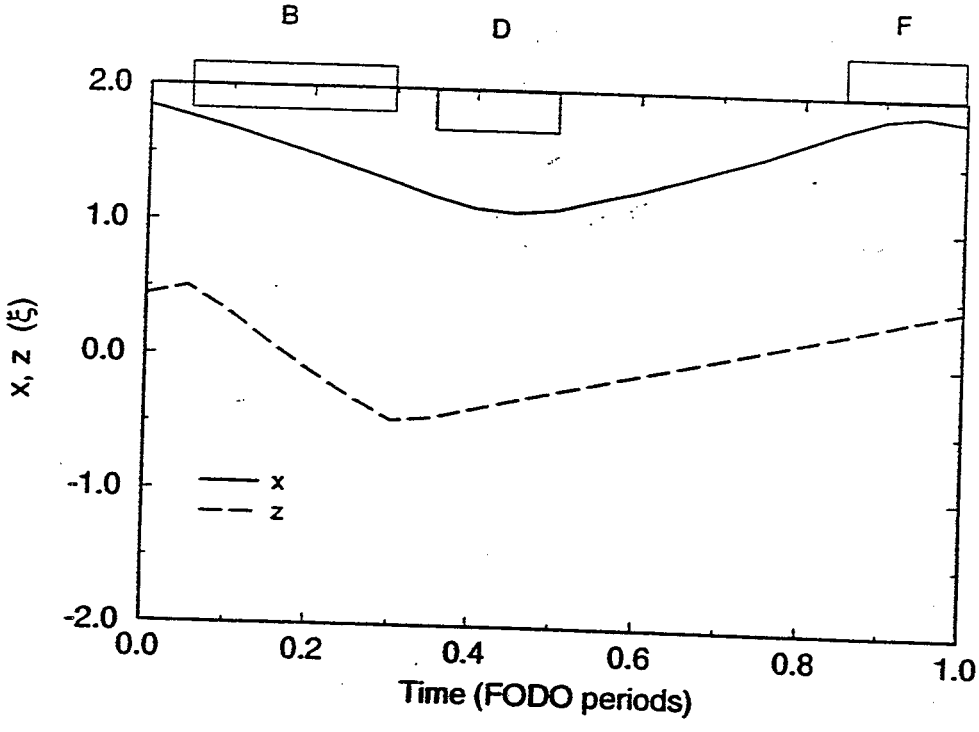

Figure 3: The effect of shear. In this study $N=40$, $L=40\xi$. Motion occurs both in the x direction (breathing) and in the z direction (shear) for a particle (with largest horizontal displacement and no vertical displacement) through a lattice cell. Lattice components are displayed on the figure, B is a bending section, F is a focusing section, D is a defocusing section. The machine parameters are the same as that used in Fig. 2, with $\gamma = 1.4$, $\nu_x = 2.8$ and $\nu_y = 2.1$.

Lattice example:

circumference 25.1 m, bending radius 1m.

superperiod = 10

$\nu_x = 2.8$, $\nu_y = 2.1$. $\gamma_t = 2.6$

beam energy $\gamma = 1.4$

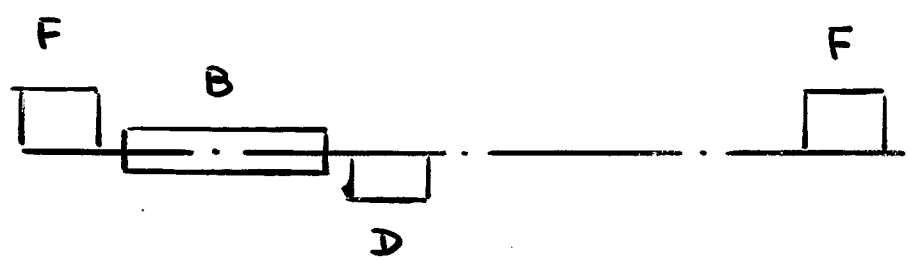

particle trajectory in one FODO period

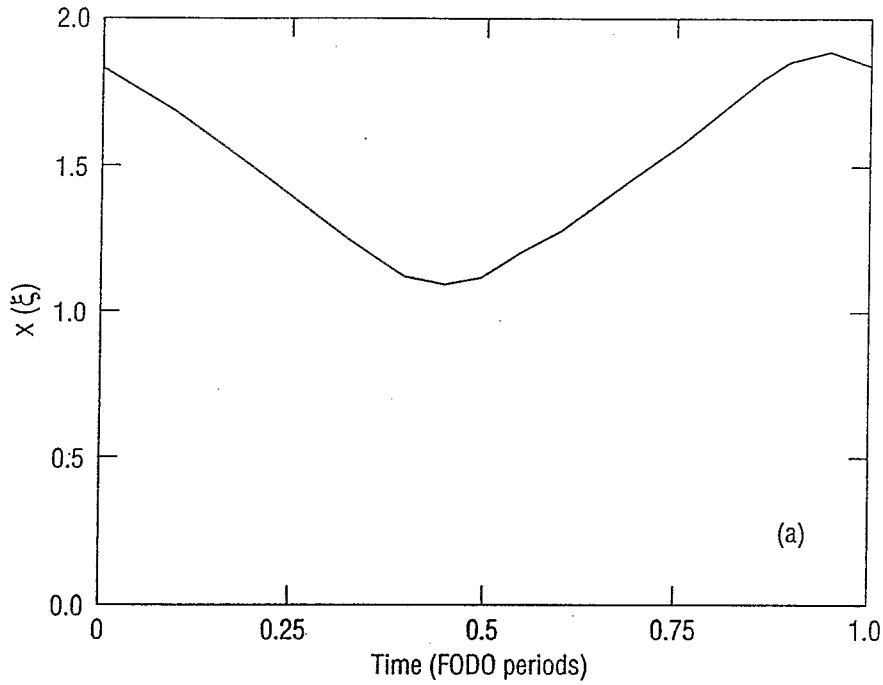

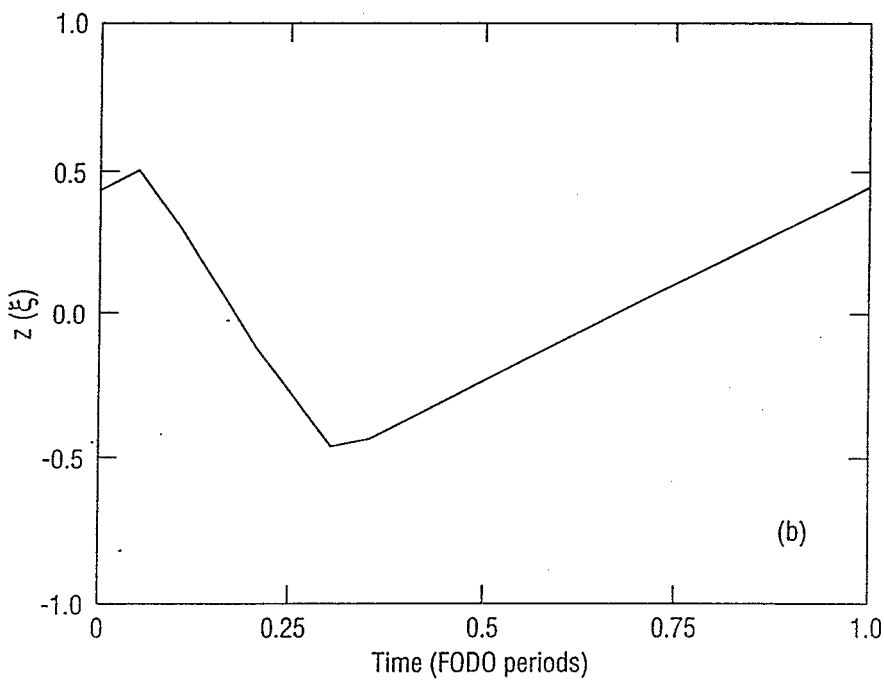

With Shear

With Shown

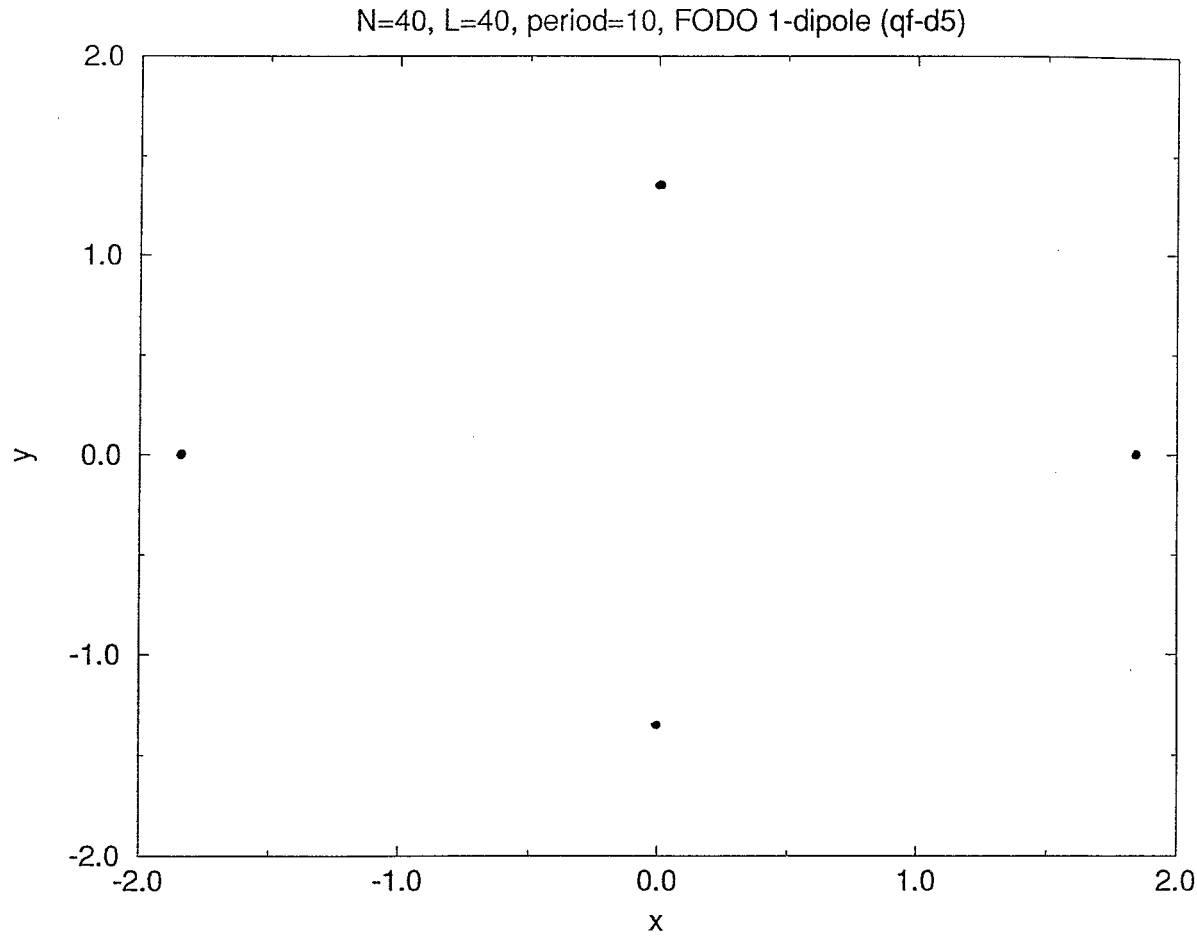
N=40, L=40, period=10, FODO 1-dipole (qf-d5)
2.0
1.0
0.0
-1.0
-2.0
y
-2.0
-1.0
0.0
1.0
2.0
x

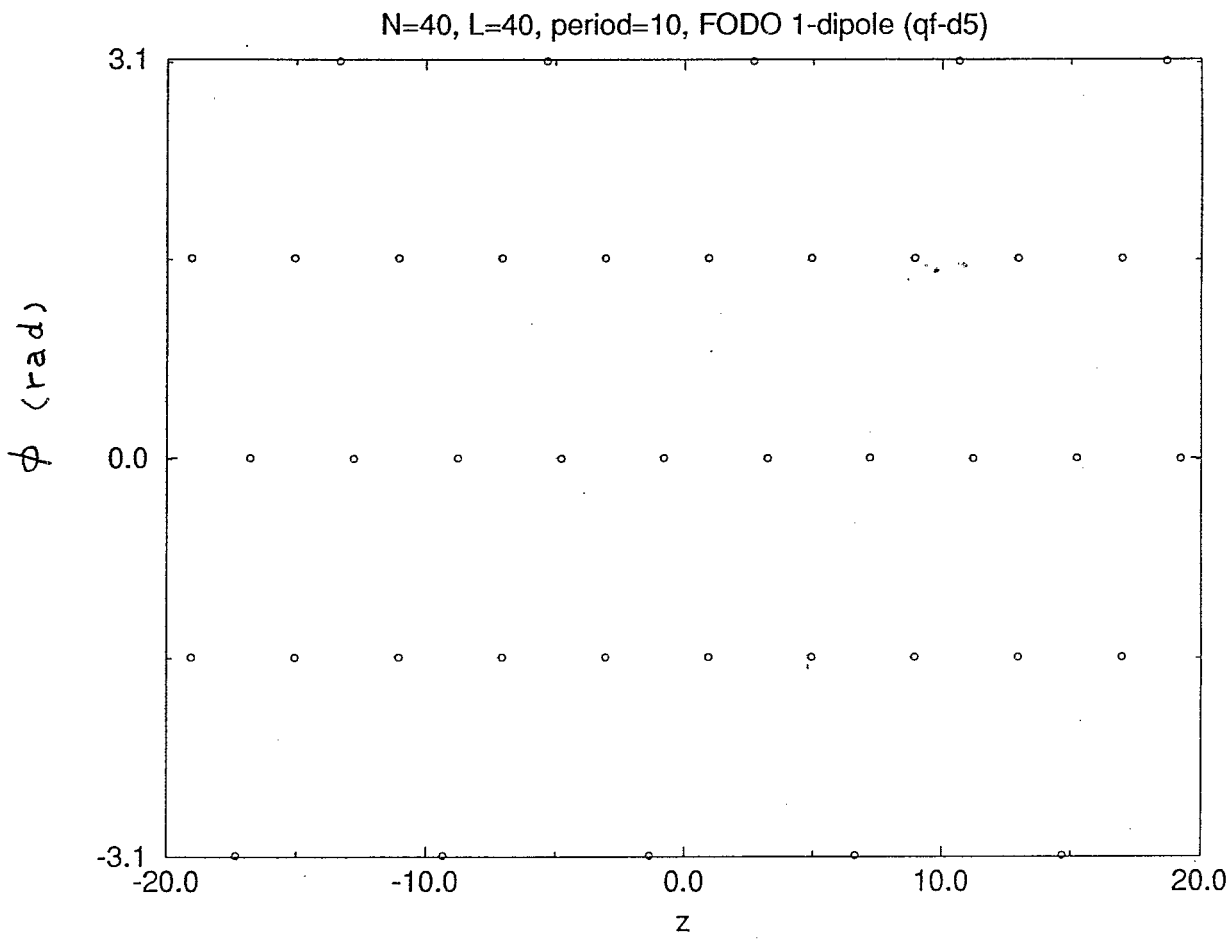
N=40, L=40, period=10, FODO 1-dipole (qf-d5)
3.1
0.0
-3.1
φ (rad)
-20.0
-10.0
0.0
10.0
20.0
z

* Crystalline structure in TSR lattice

TSR lattice, superperiodicity = 2.

$\nu_x = 2.3$, $\gamma = 1.001$ (?)

modeled with 376 steps per revolution

* low density structures has been formed

1-D string

. . . . . .

2-D zig-zag, rotating transversely

twice per revolution

. . .

. . . .

* high density structures hard to achieve

too much heating ?

too much shear ?

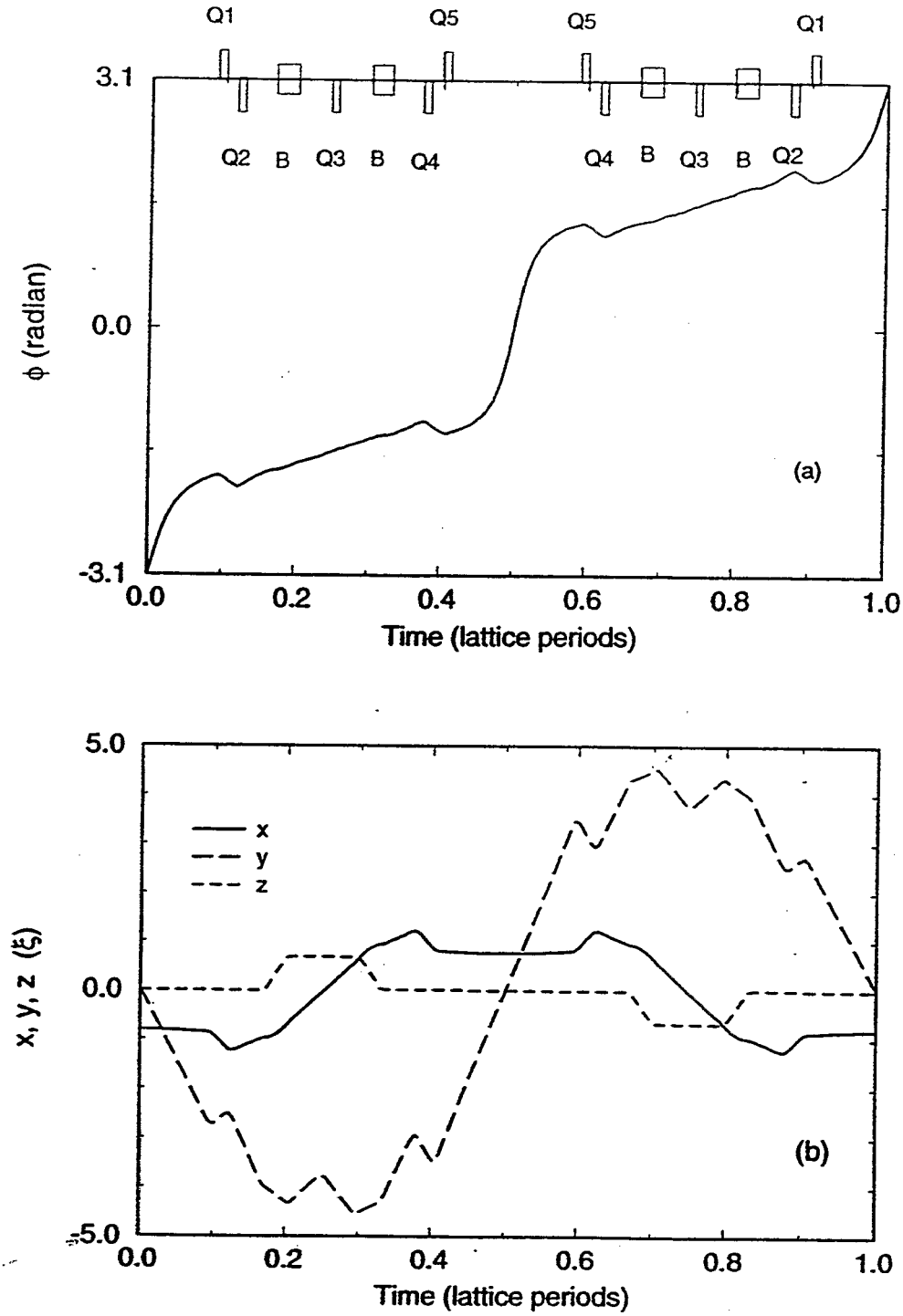

Figure 4: A zig-zag structure formed with the Heidelberg TSR machine lattice with (a) the polar angle ϕ and (b) displacements in x, y, and z of the particle changing with time during one lattice period. Lattice components are displayed on the figure, and the lattice periodicity is 2.

Condition for 1D → 2D transition

dispersion relation (smooth approximation)

$$\begin{cases} \omega_{1,3}^2(k) = \frac{1}{2}\left\{\nu_x^2 + \Omega_k^2 \pm \left[(\nu_x^2+\Omega_k^2)^2 - 8\Omega_k^2(\nu_x^2-\gamma^2-\Omega_k^2)\right]^{1/2}\right\} \\ \omega_2^2(k) = \nu_y^2 - \Omega_k^2 \end{cases}$$

$$\Omega_k^2 = 2\sum_{n=1}^{\infty} \frac{1-\cos(kn\Delta)}{n^3\Delta^3}, \qquad \Delta = \frac{d_z}{\langle\xi\rangle}\cdot\gamma$$

when

$$\nu_x^2 - \gamma^2 < \frac{4.2}{\Delta^3}$$

or

$$\nu_y^2 < \frac{4.2}{\Delta^3}$$

transverse focusing — Coulomb repulsion

1D → 2D

Dispersion relation

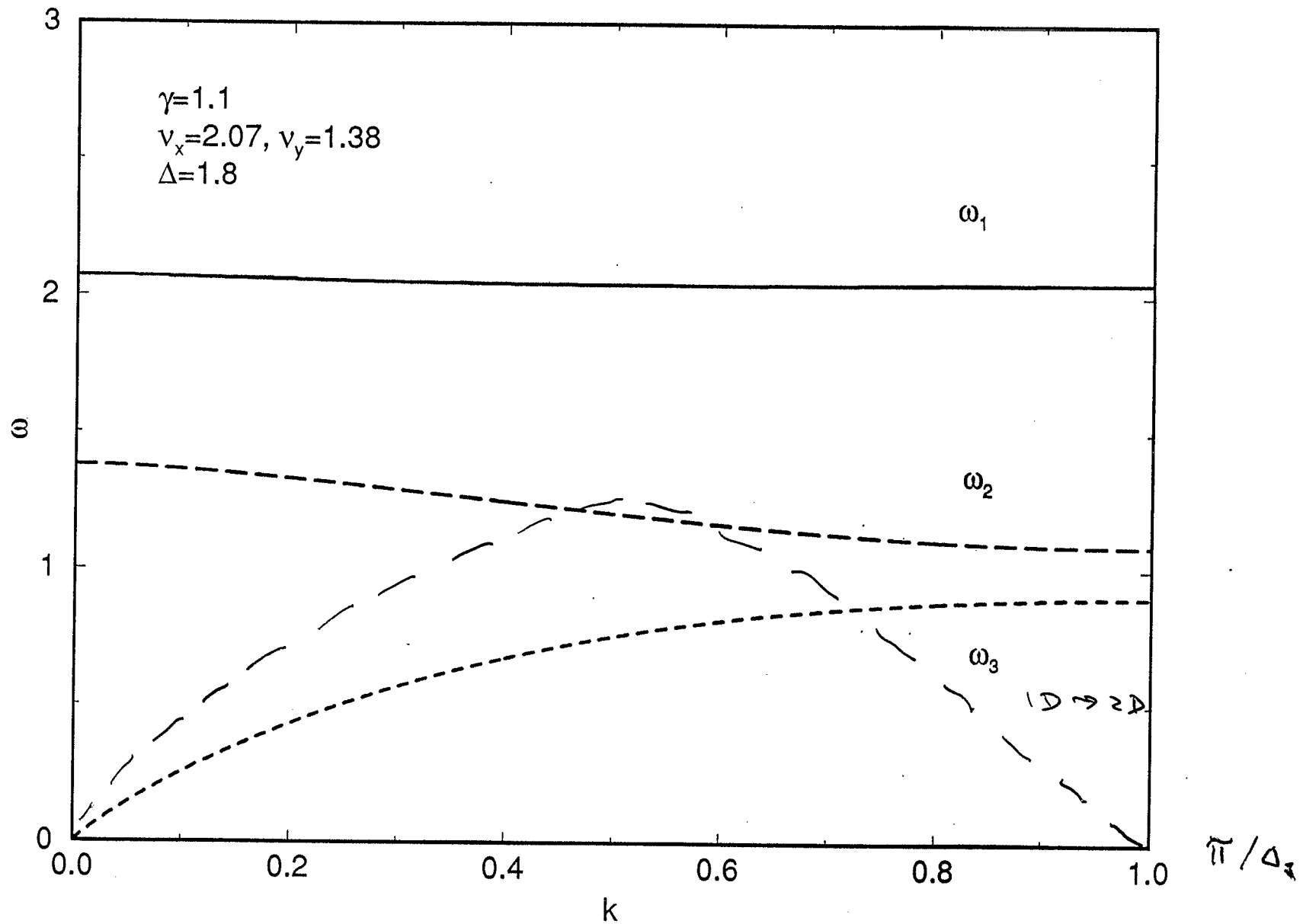

* High density limit

$$\nu_x^2 - \gamma^2 = \Omega_k^2$$

↳ ΔQ^2, incoherent tune shift

$$\Omega_k^2 = \Delta Q^2 = \rho \cdot \frac{2 r_0 R^2}{\beta^2 \gamma^3}$$

$$\boxed{\rho \leq \frac{\beta^2 \gamma^3 (\nu_x^2 - \gamma^2)}{2 r_0 R^2}} \leftarrow \nu_\gamma^2$$

With ASTRID ring, $^{24}Mg^+$, $\beta = 3 \times 10^{-3}$

$$\rho \leq 2.4 \times 10^{12} \left(\frac{1}{m^3}\right)$$

$$d = \left(\frac{1}{\rho}\right)^{1/3} \geq 75 \ \mu m$$

i.e. $$\rho_{max} \approx \frac{\gamma \nu_y \sqrt{\nu_x^2 - \gamma^2}}{2 \xi^3}$$

IV. Conditions for melting

beam frame

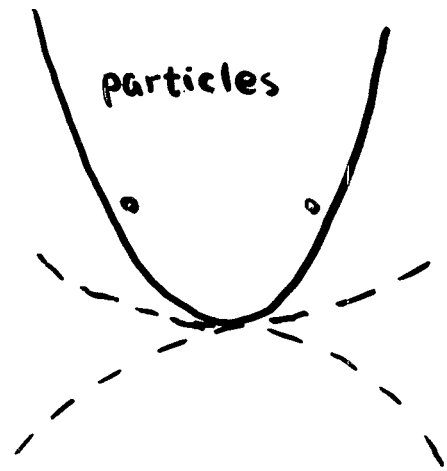

lattice potential

periodic vibration

* lattice vibration emits phonons into crystal

  ⇒ heat up, melt

* resonance condition (energy conservation)

$$\omega_{Lattice} = \omega(k_1) + \omega(k_2) + \cdots$$

↑ phonons

* define "temperature" under time-dependent environment

$$T_x = \langle \Delta P_x^2 \rangle, \quad T_y = \langle \Delta P_y^2 \rangle, \quad T_z = \langle \Delta P_z^2 \rangle$$

deviation from the ground state value
↑ periodic

* relation to emittances and momentum $\frac{\Delta p}{p}$

$$\left(\Delta \varepsilon_x, \Delta \varepsilon_y, \frac{\Delta p}{p}\right) = \left(\frac{\xi^2}{R^2} \bar{\beta}_x T_x, \frac{\xi^2}{R^2} \bar{\beta}_y T_y, \frac{\xi}{R} \gamma \sqrt{T_z}\right)$$

* determine critical T_x, T_y, T_z by calculating the correlation function under certain temperature

Survival plot

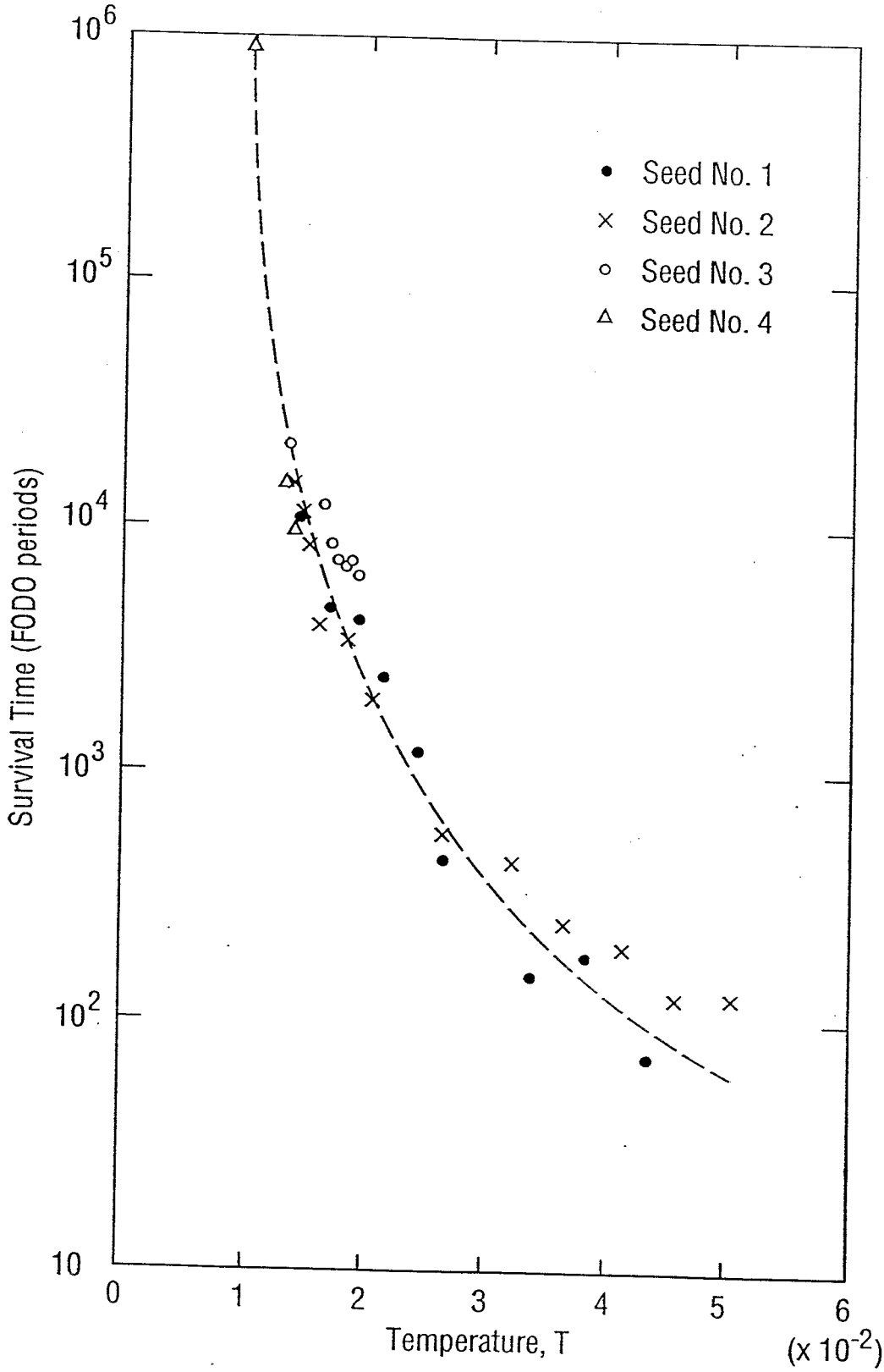

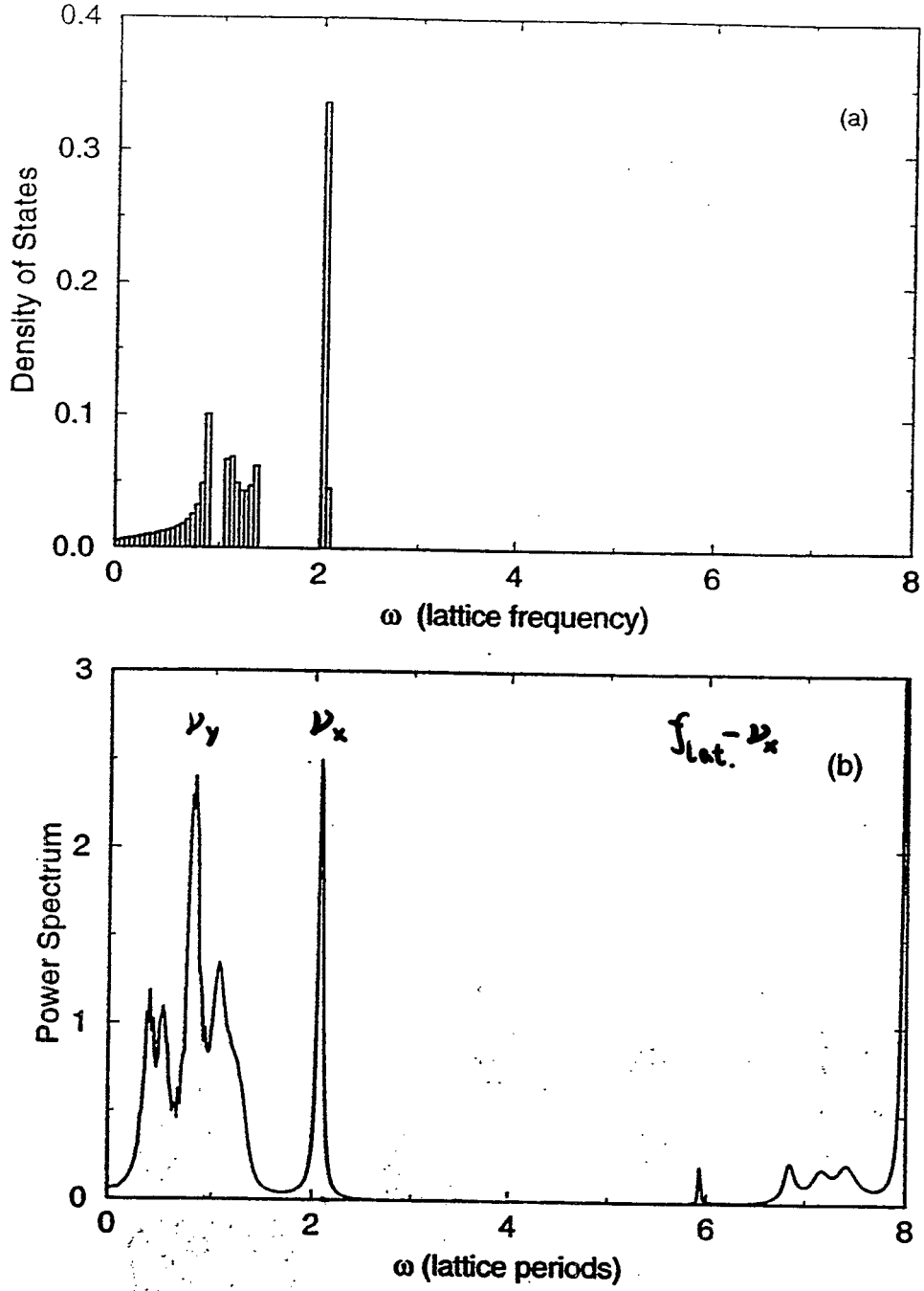

Figure 6: Vibrational density of states (a) under smooth approximation and (b) for the exact Hamiltonian from molecular dynamics (with $N=100$ and $L=180\xi$) for a 1-D chain. The machine consists of 8 lattice periods, each containing a FODO cell and an insertion (containing drift spaces and two quadrupole magnets), with $\nu_x = 2.07$, $\nu_y = 1.38$, and $\gamma = 1.1$.

* Condition for melting :

$$f_{lattice} > 2 \cdot \max(\nu_x, \nu_y)$$

for the crystal to last a meaningful time.

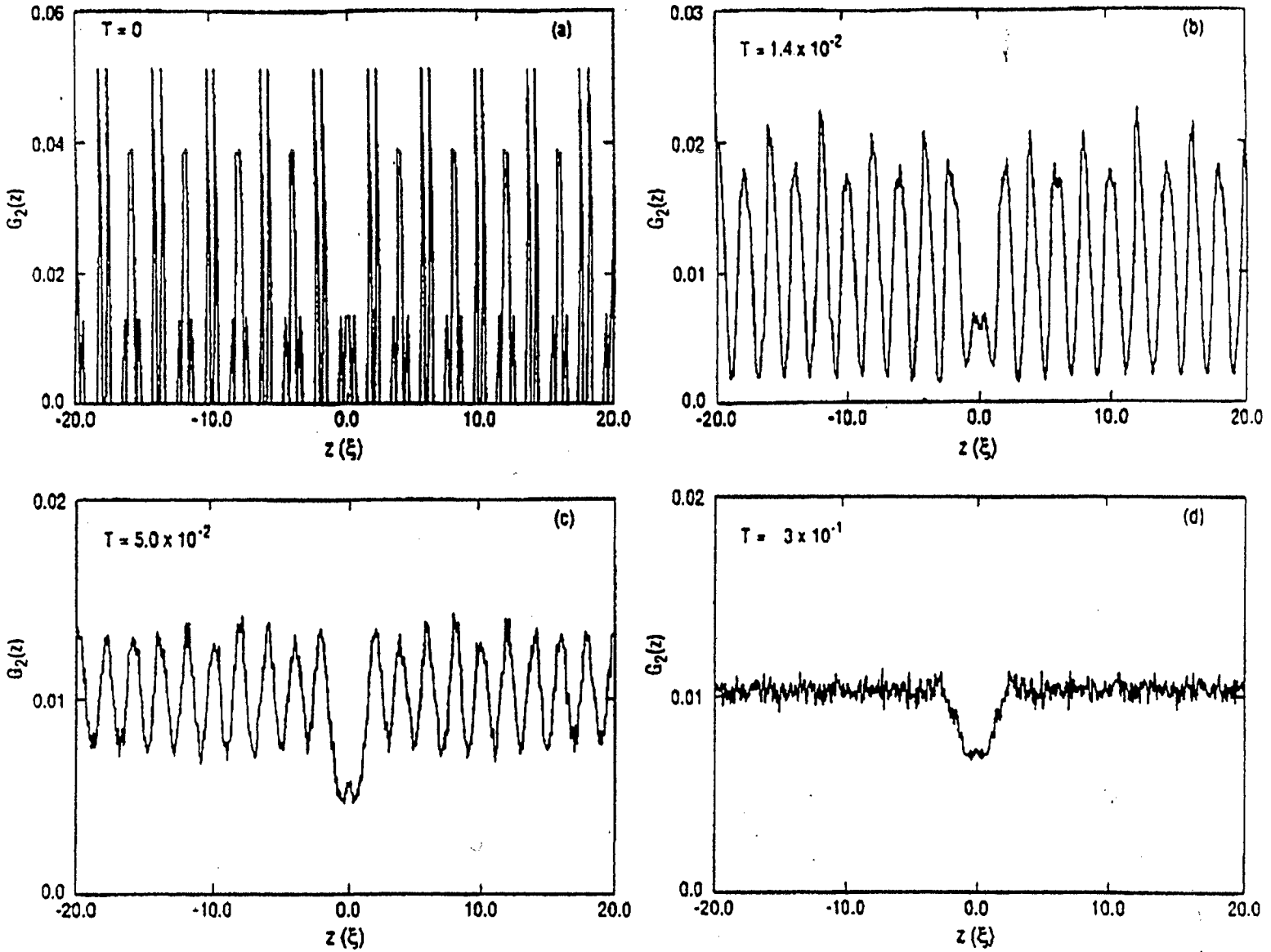

Figure 9: Two-body correlation function $G_2(z)$ at various temperatures. The machine and beam parameters are the same as that used in Fig. 7.

* scaling rules of break-up temperature

longitudinal

$$\langle P_z^2 \rangle \approx \frac{0.6}{\Delta_z}$$

kinetic energy ~ potential energy diff.

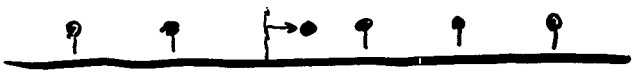

$$\omega_z^2(k) = \frac{4}{\Delta_z^3} \sum_m \frac{1}{m^3} - \frac{4}{\Delta_z^3} \sum_m \frac{\cos(m k \Delta_z)}{m^3}.$$

transverse

$$\langle P_{x,y}^2 \rangle \sim \Delta_z^2$$

$$d_x \sim \Delta_z$$

$$\omega_x^2(k) = (\mu_x^2 - \gamma^2) - \frac{2}{\Delta_z^3} \sum_m \frac{1}{m^3} + \frac{2}{\Delta_z^3} \sum_m \frac{\cos(m k \Delta_z)}{m^3}$$

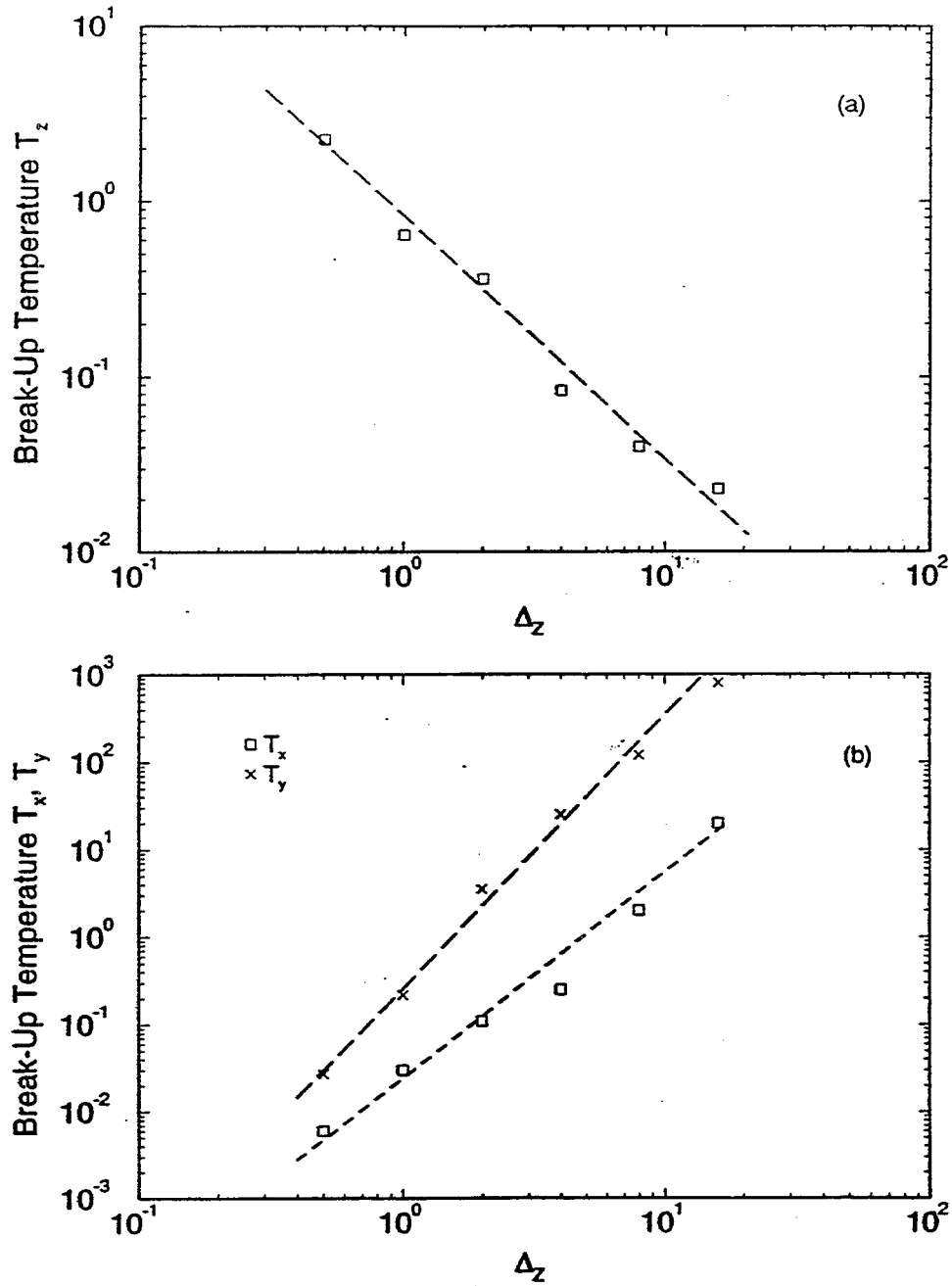

Figure 5: Break-up temperatures in the (a) azimuthal and (b) transverse direction as functions of the inverse of the beam density. The machine parameters are the same as that in Fig. 1. The result has been verified by comparing cases with different L and N (N =10, 20, 50, 100, and 200) while keeping the line density $\Delta_z^{-1} = N/L$ constant ($\Delta_z = 2$).

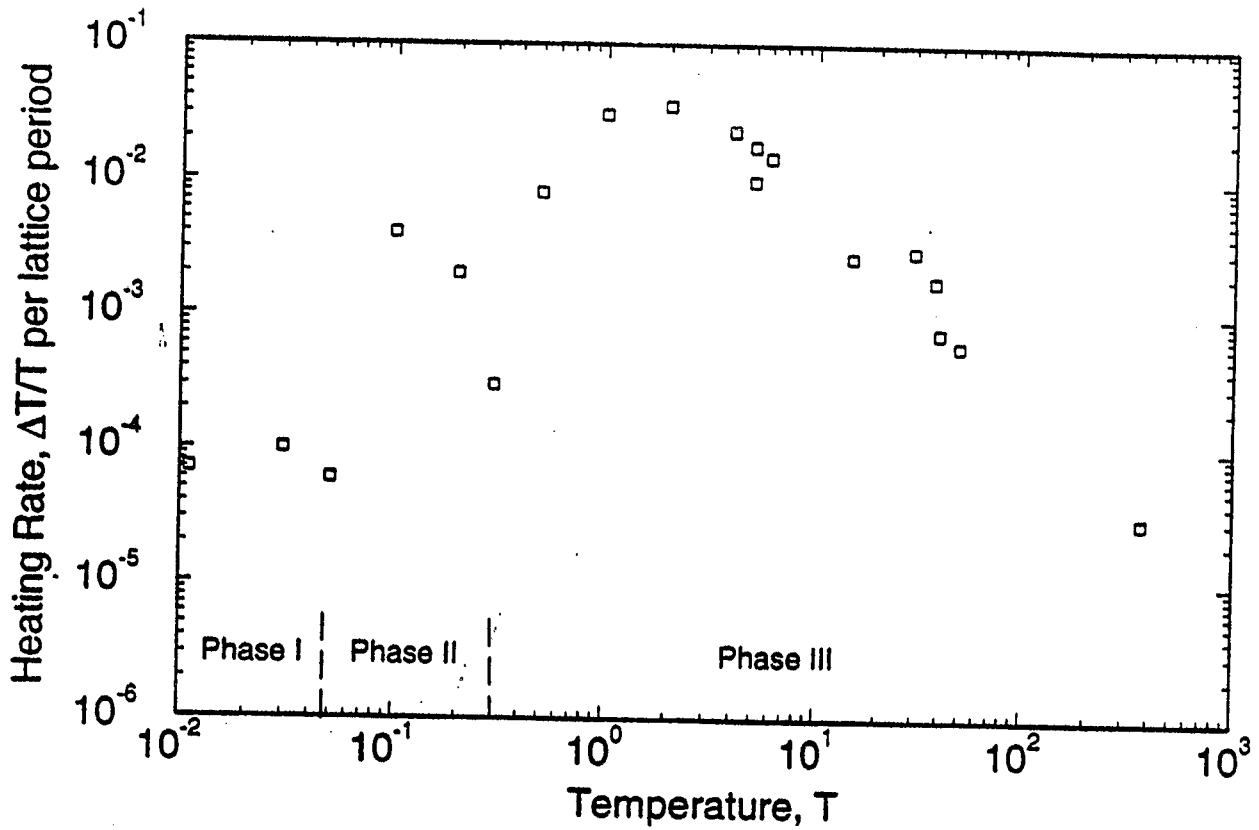

Figure 8: The heating rate as a function of the temperature T. The machine and beam parameters are the same as that used in Fig. 7. The break-up temperature is about $T \approx 0.3$.

* storage ring model

10 identical FODO cells, $n = \pm 50$

circumference = 24 meter

$\nu_x = 2.7$, $\nu_y = 2.3$, $\gamma_T = 2.5$

chosen $\gamma = 1.4$

$\bar{\beta}_x = 9$ m, $\bar{\beta}_y = 10.5$ m

$$\xi = \begin{cases} 1.8 \times 10^{-6} & \text{(proton)} \\ 2.2 \times 10^{-5} & \text{(electron)} \end{cases}$$

* condition for ordered state

$$\left(\Delta\varepsilon_x, \Delta\varepsilon_y, \frac{\Delta p}{p}\right) < \begin{cases} (0.8\times10^{-11}\, T_x,\ 0.9\times10^{-11}\, T_y,\ 1.3\times10^{-6}\sqrt{T_z}) \\ (1.2\times10^{-9}\, T_x,\ 1.3\times10^{-9}\, T_y,\ 2.1\times10^{-5}\sqrt{T_z}) \end{cases}$$

$\uparrow$ $x \to z$ $\quad$ $\uparrow$ $y \to z$ $\quad$ $\uparrow$ ordering in z

heat transfer

no crystallization possible if $\gamma > \gamma_T$

V. Conclusion

* crystalline beam can form in AGS machine when beam energy is below transition energy.
* crystals can last long if lattice periodicity is higher than twice betatron tunes.
* require careful ring design and effective cooling to achieve it.